# I. Cover Page Data Elements

**a. ARI Project:** 11129
**ARI Report No**.: RP-11129.2

**b.** DOE/Office of Science Program Office: Climate and Environmental Sciences Division

**c. DOE Award Number:** DE-SC0014287

**d. Project Title:** Understanding the Evolution of Biomass Burning Particles in the Atmosphere: Analysis of BBOP Data, Laboratory Experiments, and Model Integration

**e. PD/PI:** Dr. Leah R. Williams, Principal Scientist, Phone: 978-663-9500 x 221, E-mail: Williams@aerodyne.com

**f. Submitting Official**: Ms. Carolyn Fialkowski, Phone: 978-663-9500 x 242, E-mail: cski@aerodyne.com

**g. Submission Date:** October 31, 2018

**h. DUNS Number**: 0308172900000

**i. Organization:** Aerodyne Research, Inc., 45 Manning Rd., Billerica, MA 01821

**j. Project Period:** August 1, 2015 to July 31, 2018

**k. Reporting Period End Date:** July 31, 2018

# Understanding the Evolution of Biomass Burning Particles in the Atmosphere: Analysis of BBOP Data, Laboratory Experiments, and Model Integration

Aerodyne Research, Inc.
45 Manning Rd., Billerica, MA 0182

Final Report
Reporting Period: 8/1/2015 to 7/31/2018
DOE Award Number: DE-SC0014287

**PI:** Dr. Leah R. Williams, Principal Scientist
Phone: 978-663-9500 x 221, E-mail: Williams@aerodyne.com

**Co-Investigators:**
Dr. Timothy Onasch and Dr. Douglas Worsnop, Aerodyne Research, Inc.
Dr. Robert Yokelson, University of Montana
Dr. Peter Buseck, Arizona State University

**Unfunded Collaborators:**
Dr. Arthur J. Sedlacek, III, Brookhaven National Laboratory
Dr. Rahul Zaveri, Pacific Northwest National Laboratory
Dr. Qi Zhang, University of California, Davis
Dr. Kouji Adachi, Meteorological Research Institute, Tsukuba, Japan

**Prepared for**:
Dr. Shaima Nasiri
U.S. Department of Energy
SC-23.3 / Germantown Building
1000 Independence Avenue, S.W.
Washington, DC 20585-1290

# II. Accomplishments

**a. Goals of Project**

Submicron particles in the atmosphere can have a profound influence on Earth's climate [*Stocker et al.*, 2013]. Particulate matter (PM) affects climate via both direct effects (scattering or absorption of radiation) and indirect effects (changes to the formation and properties of clouds). Biomass burning (BB) is the largest global source of submicron, carbonaceous particles [*Wiedinmyer et al.*, 2011]. Field campaigns have shown that BB aerosol (BBA) can evolve through rapid transformations and removal processes in the atmosphere, with changing radiative and hygroscopic properties, but these processes are not well characterized. Better understanding of the evolution of biomass burning PM in the atmosphere is critical for improving the accuracy of regional to global climate models.

In order to address uncertainties in the initial physical, chemical and radiative forcing of BBA and the evolution of these parameters, DOE ASR conducted an airborne field campaign, the Biomass Burning Observation Project (BBOP), during the summer and fall of 2013 to make measurements in the plumes of northwest U.S. wildfires and southeast U.S. agricultural burns. BBOP provided unique, extremely detailed trace gas and particle measurements in fresh biomass burning plumes and captured large, rapid downwind transformations within a few hours of the sources. These fast changes in properties have also been observed in laboratory-generated BB smoke in a smog chamber, but in general the controlling factors and most likely outcomes in the real atmosphere are still not clear.

The goals of this project were to 1) analyze and interpret the BBOP measurements in detail, 2) conduct laboratory experiments to explore the formation of tar balls, and 3) to incorporate our findings into improved models of biomass burning emissions and aging. This research focuses on understanding the chemical, physical and optical properties and transformations of BB emissions in the near-field within hours downwind of the burn and on a more regional scale and, in turn, how BB emissions relate to climate forcing. Analysis of the BBOP data paid particular attention to relating SOA production, changes in size distribution, and mixing state to the environmental conditions (gas-phase precursors, relative humidity, radiation, oxidants, $NO_x$, etc.).

This project included subcontracts and unfunded collaborations with many of the key participants in the BBOP campaign. Professor Robert Yokelson at the University of Montana is an expert on biomass burning fuels and emissions and participated in BBOP as an unfunded collaborator. Professor Peter Buseck at Arizona State University collected particle samples during BBOP and analyzed some of them as part of this project. Unfunded collaborators include Dr. Arthur Sedlacek, III at Brookhaven National Laboratory (BNL) and Dr. Rahul Zaveri at the Pacific Northwest National Laboratory (PNNL) who were both principal investigators in the BBOP campaign, focusing on measurements and modeling, respectively. We are also working closely with Prof. Qi Zhang at UC Davis to coordinate analysis of BBOP flight data and data from the Mt. Bachelor Observatory (MBO), and with Dr. Kouji Adachi at the Meteorological Institute (Japan) to analyze laboratory-generated tar ball samples.

**b. Accomplishments**

During the first year of this project, we focused most of our time and energy on extending the analysis of the chemical and optical data from various instruments flown on the G1 during BBOP, with specific emphasis on the Aerodyne Research, Inc. Soot Particle Aerosol Mass Spectrometer (SP-AMS) and Cavity-Attenuated Phase-Shift (CAPS) particulate extinction

($PM_{EX}$) monitor. For the SP-AMS, this analysis focused on better quantifying and separating the refractory black carbon ion signals from the organic ion signals and characterizing the chemical properties of the organic component, including oxygen-to-carbon ratios, oxidation states, and specific chemical markers. In addition to the SP-AMS, we analyzed chemical and physical information about refractory Black Carbon (rBC) from the Soot Particle Soot Photometer (SP2) and Transmission Electron Microscopy (TEM) images. In addition to the CAP $PM_{EX}$, we analyzed optical measurements from the nephelometer, the Photo-Thermal Interferometer (PTI) developed by Dr. Sedlacek at BNL, the 355 nm Photo Acoustic Spectrometer (PAS) developed by Dr. Arnott (UN-Reno), and PSAP filter-based transmission measurements. During this process, we worked closely with Drs. Sedlacek and Kleinman from Brookhaven National Laboratory (BNL), Dr. Buseck (ASU), and Dr. Zhang (UC Davis) and her research group.

During the second and third years of this project, we worked on publishing the results of the analysis of the BBOP field campaign data and we also conducted a laboratory experiment designed to generate and measure tar balls. In addition, we performed laboratory experiments to better understand the SP-AMS measurements made when both the tungsten and laser vaporizers are present in the ionization region (the condition during the BBOP campaign). We had preliminary discussions with Dr. Zaveri at PNNL about incorporating the experimental results into atmospheric models, but did not progress to the stage of developing new MOSAIC modules to incorporate our better understanding of biomass burning particle emissions.

Highlights from the project include:

1. Characterization of the influence of biomass burning particles on a regional level using high resolution Aerosol Mass Spectrometer (HR-AMS) measurements from the G1 compared with similar measurements conducted at the Mount Bachelor Observatory (MBO) site showed that the regional BB aerosol is strongly influenced by the modified combustion efficiency (MCE) of the wildland fires sampled. For example, the organic aerosol mass loading relative to carbon monoxide is a stronger function of the measured MCE than distance from the burns, whereas the organic chemical information (i.e., oxidation states) are influenced by both the MCE and downwind distance. This work has been published in ES&T [*Collier et al.*, 2016].
2. Transmission Electron Microscopy (TEM) observations of biomass burning aerosol explicitly show the rapid formation and evolution of tar balls downwind in wildland fires, but not agricultural burns. Biomass burning particles are observed to change morphology from low viscosity particles that spread across TEM grids to well-defined spherical tar balls. Combining TEM images with chemical information from the SP2 and SP-AMS enables the first estimates of tar ball mass fractions in biomass burning emissions. This work has implications for the assumption that tar balls are primary emissions from biomass burns. This work has been published in Atmospheric Chemistry and Physics [*Sedlacek et al.*, 2018a]. A second paper is in preparation for Nature Geoscience [*Adachi et al.*, 2018].
3. Capitalizing on the first flights of a new 355 nm Photo-Acoustic Spectrometer (PAS) developed and flown by Dr. Arnott (UN Reno), we observed absorbing organic aerosol (termed Brown Carbon or BrC) formation and evolution in biomass burning plumes downwind from wildland fires. Combining these measurements with other optical and chemical measurements provide an estimate of primary and secondary BrC emission and

formation from wildland fires. These results are in preparation for Atmospheric Chemistry and Physics [*Sedlacek et al.*, 2018b].

4. The chemical properties of biomass burning particles as measured by AMS and SP-AMS instruments, and combining with other chemical and optical measurements, are being analyzed by Aerodyne, led by Dr. Onasch and UC Davis, led by Dr. Zhang. These detailed analyses investigated the thermal volatility of the biomass burning particles (at MBO), Positive Matrix Factorization (PMF) analyses of AMS data collected at MBO and the G1 for insights into chemical processing, and correlations with simultaneous optical and physical (i.e., size distributions and TEM images) measurements. These results were published in Atmospheric Chemistry and Physics [*Zhou et al.*, 2017]. A second paper is in preparation [*Onasch et al.*, 2018].
5. Professor Yokelson led a team of scientists that calculated emission factors (EF, g/kg of dry fuel burned) for gas-phase and particle-phase emissions from some of the BBOP sampled fires. These results will lead to improved air quality models. These results were published in the Journal of Geophysical Research: Atmospheres [*X Liu et al.*, 2017].
6. We generated tar balls in the laboratory via pyrolysis of pine needles and twigs and sampled them with the SP-AMS, SP2 and TEM grids. Analysis of the TEM grids confirmed the presence of tar balls. Analysis of the SP2 data suggested that significant charring of tar balls can occur in the SP2 detection process. This result suggests that ambient measurements of black carbon with the SP2 may be overestimated [*Sedlacek et al.*, 2018c].
7. We characterized and mitigated an issue with the SP-AMS where turning the SP laser on and off leads to erroneous measurements of organic mass loading due to heating of internal SP-AMS components. This result will improve the interpretation of field measurement data, such as in BBOP, and will lead to modifications of the SP-AMS instrument.

These findings have resulted in 5 publications in archival journals, 1 book chapter, and another 4 manuscripts in preparation. The results have been presented at international meetings (2015 and 2017 European Aerosol Conference, 2015 International Conference on Carbonaceous Particles in the Atmosphere, 2017 and 2018 American Geophysical Union Annual Meeting, 2017 American Association for Aerosol Research Annual Conference, and 2018 International Aerosol Conference) and DOE ASR/ARM PI meetings (2015, 2016, 2017 and 2018). Details about publications and presentations are given in Section d. Dissemination of Results.

**Accomplishments by Task**

**Task 1. Analysis of Biomass Burning Observation Project (BBOP) Data (Years 1 and 2)**

The first phase of this project was intensive analysis of field data obtained onboard the ARM Aerial Facility (DOE ARM Gulf Stream = G1) during flights through biomass burning plumes (both forest fires and agricultural burning) as part of the BBOP campaign during the summer and fall of 2013. Figure 1 shows G1 transects of the plume from the 28 Mile Marker fire on 7/26/2013 and illustrates the kind of information targeted in the BBOP campaign. The right panels suggest rapid SOA formation in the first few hours of the plume. This project focused on a much more detailed characterizations of the sampled plumes' evolution across the entire BBOP dataset.

Aerodyne provided and operated a soot particle aerosol mass spectrometer (SP-AMS), which provides unprecedented new details about BC containing particles, and a cavity-attenuated phase shift (CAPS) extinction monitor (PMEX) during BBOP with DOE ARM funding. BBOP represented the first airborne deployments of these instruments. In addition to these new technologies, the BBOP study also included several other new or recently developed instruments on-board the G1 in order to benefit from state-of-the-art measurements, including the Photo-Thermal Interferometer (PTI) developed by Dr. Sedlacek (BNL), a 355 nm Photo-Acoustic Spectrometer (PAS) developed by Dr. Arnott (UN-Reno), and the Fast Integrated Mobility Spectrometer (FIMES) developed by Dr. Jian Wang (BNL). Table 1 details the particle optical measurements and Table 2 details the particle chemical and physical measurements from the G1.

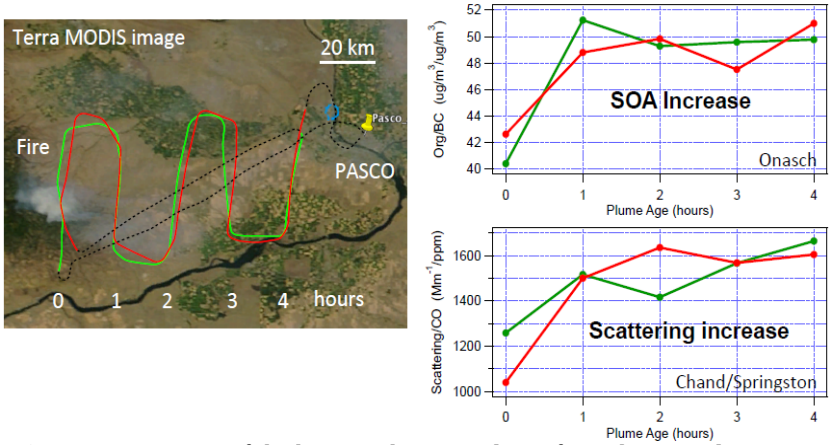


**Figure 1.** Transects of the biomass burning plume from the 28 Mile Marker fire during BBOP on 7/26/2013. (Left panel) Flight path of G-1. (Right panel, top) Ratio of organic mass loading to rBC mass loading measured with SP-AMS indicating the rapid increase in SOA with plume age. (Right panel, bottom) Increase in optical scattering with plume age due to increase in SOA. Red and green lines in all 3 panels refer to two different flight paths.

**Table 1. Optical Properties Measured on the G-1**

| **Optical Measurement** | Instrument | Wavelength(s) |
|---|---|---|
| Extinction | 1-λ CAPS PMEX | 630 nm |
| Scattering | 3-λ Nephelometer | 450, 550, 700 nm |
| Absorption | 1-λ PAS | 355 nm |
| | 1-λ PTI | 532 nm |
| | 3-λ PSAP | 462, 523, 648 nm |

**Table 2. Chemical and Physical Properties Measured on the G-1**

| **Measurements** | Instruments |
|---|---|
| Non-Refractory Particulate Matter (NR-PM) | SP-AMS, TEM |
| Refractory Black Carbon (rBC) | SP2, SP-AMS, TEM |
| Size | UHSAS, PCASP, FIMS |

A significant fraction of the instruments on-board the G1 during BBOP were operated with 1 second data collection, enabling highly detailed analyses of the varied plumes sampled by the G1 in flight, which could last from a few seconds, for concentrated smoke plumes near fires, to minutes and longer for diluted plumes downwind from fires and urban centers. In order to analyze combined data sets from multiple different instruments, we have to correlate the different sampling times (typically differing by seconds due to different computer times and

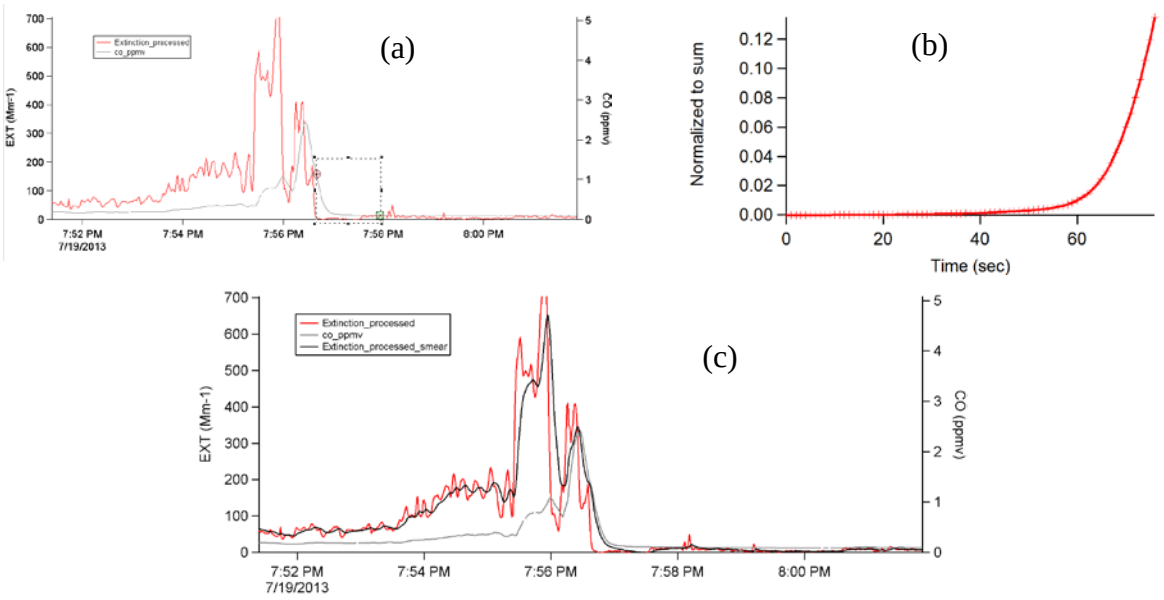


**Figure 2.** (a) Measurements of particle extinction and [CO] as a function of sampling time with a ~ 1ppmv [CO] drop in middle of time period highlighted by marquee box. (b) Shows the CO-specific time response function used to smooth or smear other data into a similar time response as the CO measurements. (c) Measurements of particle extinction smeared using the CO-specific time response function, compared with the [CO] measurements, showing very good second-by-second correlation.

sampling inlet transfer times) and sampling time response (i.e., how long it takes a sample of air to clear out of an instruments sampling volume). These tasks are not part of any given instrument's QA/QC process, and only become relevant and important when integrating multiple instrument measurements.

### 1.1 Modified Combustion Efficiency

Modified combustion efficiency (MCE) is used to estimate the relative amount of smoldering to flaming in a biomass burning event. MCE is defined as the ratio of the change in $CO_2$ above background to the combined change in CO plus $CO_2$ above background, MCE = $\Delta CO_2 / (\Delta CO + \Delta CO_2)$ [*Lobert et al.*, 1991; *Yokelson et al.*, 1996]. An MCE greater than 0.9 is associated with more flaming combustion, while MCE < 0.9 is associated with more smoldering combustion. Previous studies have demonstrated that the amount of particulate matter and gas-phase emissions are strongly influenced by MCE [*Akagi et al.*, 2013; *Burling et al.*, 2011; *McMeeking et al.*, 2009; *Yokelson et al.*, 2011].

The first step in determining the MCE is to place both the $CO_2$ and CO measurements on the same time base. During BBOP, the CO measurements exhibited an approximately 7 second sampling time response. In order to correlate all other measurements to CO, specifically in this case the $CO_2$, we need to effectively smear the other data (i.e., $CO_2$) using a CO-specific time response function. To generate the CO-specific time response function, we need to find a rapid increase or drop in CO concentrations. Figure 2a shows a ~ 1 ppmv drop in CO concentrations after exiting a biomass burning plume, followed by a period of low CO concentrations. This data drop is cut out, inverted in time, and normalized to the sum of the CO signal. The resulting time response function for the CO measurements is shown in Figure 2b. This function is then applied to other measurements, such as the particulate extinction measurements shown in Figure 2c, enabling nearly second-by-second correlation between two different measurements.

## 1.2 Particulate Optical Properties

### *1.2.1 CAPS Extinction Monitor Data Analysis*

Aerodyne Research, Inc. has developed several aerosol optical instruments, with DOE SBIR funding, based on our proprietary Cavity Attenuated Phase Shift (CAPS) technology, including a particle extinction monitor (CAPS $PM_{EX}$) [*Massoli et al.*, 2010], a 3-λ particle extinction monitor (CAPS $PM_{EX}$-3) that was recently deployed at the DOE ARM Southern Great Plains (SGP) supersite, and a particle single scattering albedo (SSA; single scattering albedo = scattering/extinction) monitor (CAPS $PM_{SSA}$) for measuring optical extinction and scattering [*Onasch et al.*, 2015b]. The CAPS instruments can cover the visible light spectrum (405 – 870 nm), allowing characterization of the wavelength dependence of the optical properties of carbonaceous particles and allowing wavelength-matching with other optical instruments. During BBOP, we deployed a CAPS $PM_{EX}$ operating at 630 nm for the first research flights by a CAPS-based optical monitor.

### *1.2.2 Extinction-to-Carbon Monoxide Ratios*

One measurement for characterizing particulate emissions and ambient states can be obtained by taking the ratio of particulate extinction (measure of the total interaction of light with particles, equals sum of scattering and absorption) or scattering to average carbon monoxide concentrations (i.e., EXT-to-CO or SCAT-to-CO). As [CO] has a long atmospheric lifetime, it can be used as a tracer for tracking how biomass burning plumes dilute in the atmosphere. Figure 3a shows average EXT plotted versus the average [CO] for the Colockum Tarps Fire sampled in the afternoon of 7/30/2013 and colored by time downwind from the fire. The range from this one fire goes from 400 to 850 $Mm^{-1}$/ppmv CO. Figure 3b shows a histogram from 8 wildland fires showing the range of average plume measurements for the EXT-to-CO ratio and comparing these to aged biomass burning plumes and urban plumes sampled during the 2014 FRAPPE study near Denver CO [*Dingle et al.*, 2016]. Continued exploration of the EXT-to-CO ratios for all fires sampled during BBOP, including wildland and agricultural, and for the multiple urban plumes sampled will provide insights into how this ratio changes from source to downwind receptor locations and how it compares with ratios measured in urban environments.

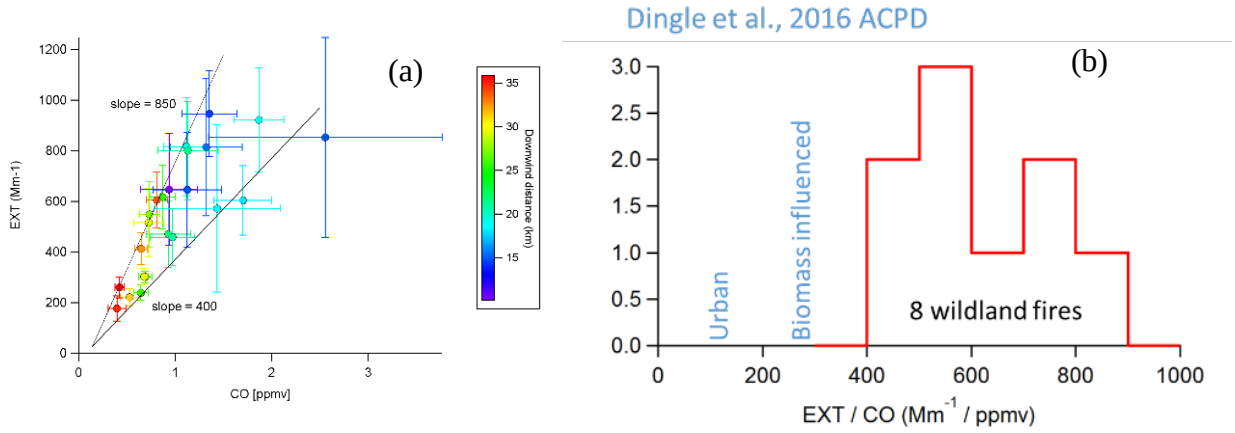


**Figure 3.** (a) Average particle extinction plotted versus average carbon monoxide concentrations for plumes sampled during the Colockum Tarps Fire and colored by distance downwind from fire. (b) Histogram of EXT/CO ratios for 8 wildland fires compared with recent urban and diluted/aged biomass burning plumes.

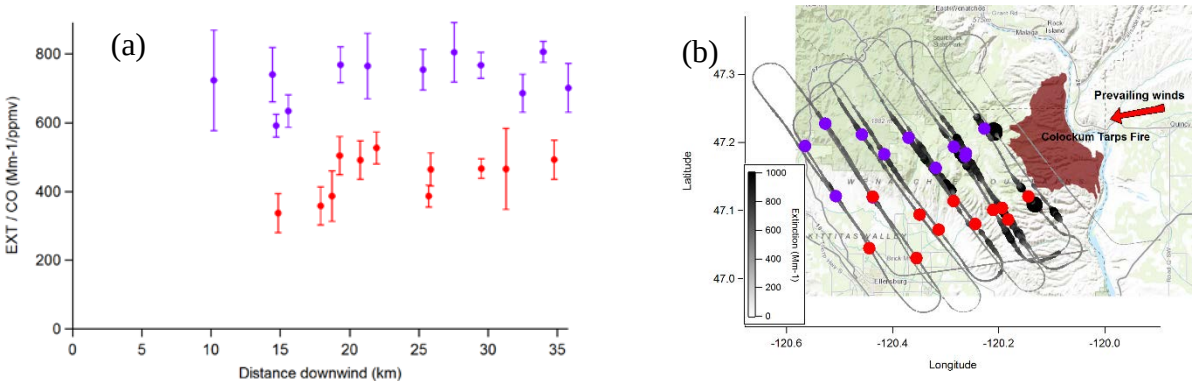


**Figure 4.** (a) Same average EXT-to-CO ratios at 630 nm shown in Figure 3a shown here as a function of downwind location from the Colockum Tarps Fire. (b) Map of same EXT-to-CO measurements plotted on the G-1 flight track, red and purple colors indicating optical properties of two different fire fronts within the overall plume.

The EXT-to-CO ratio can also be used to characterize different burn conditions within a single fire plume. Figure 4 shows the same average EXT-to-CO ratios at 630 nm as shown in Figure 3a as a function of (a) distance downwind from the burn and (b) along the G-1 flight path during measurements of the Colockum Tarps Fire in the afternoon of 7/30/2013. The red and purple colors indicate different parts of the plume which have different optical properties. The red symbols show lower EXT-to-CO ratios which increase with increasing distance from the fire, while the purple symbols show higher EXT-to-CO ratios which is relatively constant with distance downwind.

*1.2.3 Single Scattering Albedos*

Particulate extinction is the sum of the scattering and absorption of light by particles. The single scattering albedo (SSA) is the ratio of the scattering to the total extinction, and thus a measure of the relative importance of scattering of light compared with absorption. The SSA is one of the key parameters for determining the direct radiative forcing of aerosol particles. Since the single scattering albedo is defined as the ratio of scattering to extinction, it can be determined from any combination of two of the three measurements (extinction, scattering and absorption). During BBOP, the SSA can be obtained at two different wavelengths, by combining the measurements from three independent instruments. The SSA at 630 nm is obtained by interpolating the scattering at 630 nm from the measured scattering at 550 and 780 nm using the integrating nephelometer (Table 1) and taking the ratio of scattering to extinction measured by the CAPS $PM_{EX}$. The SSA at 532 nm is obtained by interpolating the

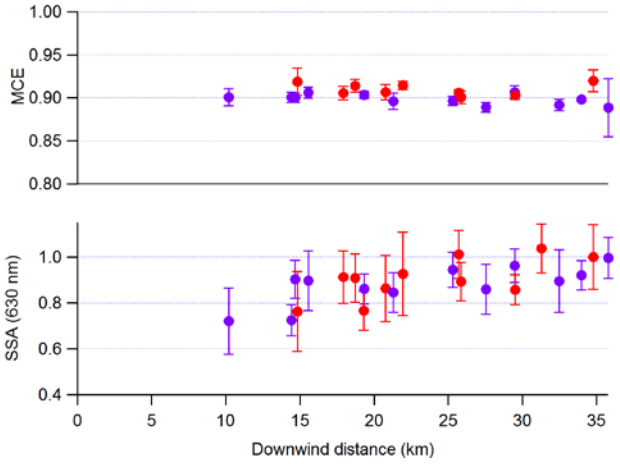


**Figure 5**. Modified combustion efficiency (MCE) and single scattering albedo (SSA) as a function of downwind distance for transects of the Coluckum Tarps Fire.

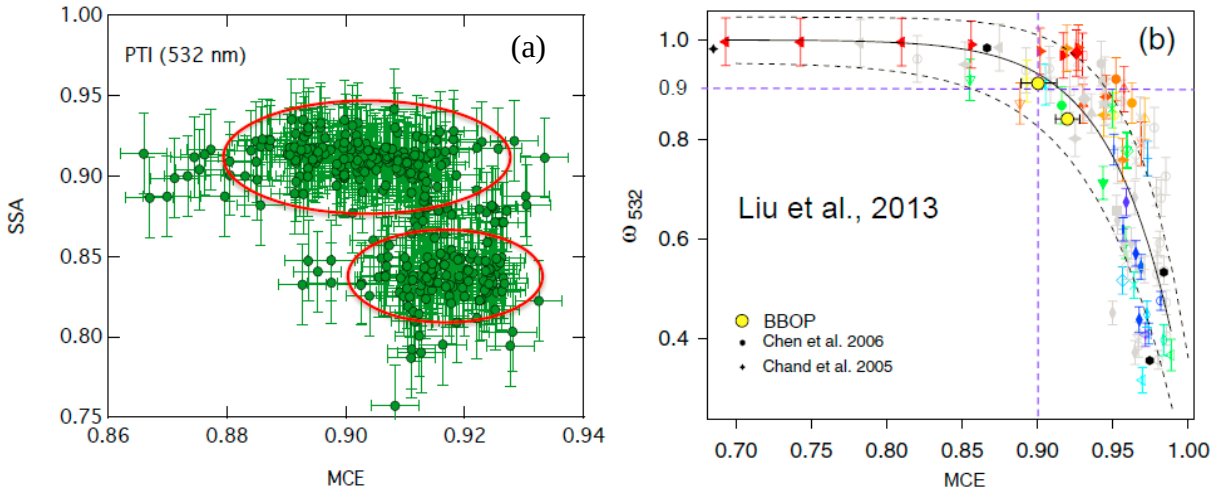


**Figure 6.** (a) SSA at 532 nm measured using the PTI and NEPH plotted versus measured MCE values. (b) Average points from (a) compared with compiled laboratory and field observations.

scattering to 532 nm from the measured scattering at 450 and 550 nm using the integrating nephelometer and taking the ratio to scattering plus absorption at 532 nm from the PTI.

Figure 5 (lower panel) shows the measured SSA at 630 nm for the Colockum Flats fire for the same G-1 transects shown in Figure 4. The SSA increases with downwind distance, indicating that scattering is increasing faster than absorption with aging of the biomass burning aerosol plume, possibly related to changes in chemical composition discussed in the next section (i.e., refractive index), morphology, or size. In contrast to the EXT-to-CO ratios in Figure 4, the SSA are the same within error bars for the two distinct plumes, indicating that in spite of optical differences, the impact on radiative forcing is similar. Figure 5 (upper panel) shows the MCE for the Colockum Flats Fire transects. The purple symbols have a slightly lower MCE than the red symbols, indicating that the northern part of the fire may have had more smoldering characteristics. This is consistent with the higher extinction shown in Figure 4 because smoldering fires emit more particulate matter with a larger size distribution.

Figure 6 shows a comparison of the SSA at 532 nm versus measured MCE values for one research flight (panel a). The average values for the two clusters of points in the red circles are compared with a compilation of laboratory and field observations in panel b [*S Liu et al.*, 2014].

*1.2.4 MAC and AAE*

Other important optical property measurements investigated during BBOP include the Mass-specific Absorption Coefficient (MAC) and the Absorbing Angstrom Exponent (AAE). The MAC ($m^2/g$) measurements are obtained by taking the ratio of the measured absorption at 355 nm (PAS) and 532 nm (PTI) to the measured rBC mass loadings by the SP2 and SP-AMS. The AAE is derived by taking the ratio of the log of absorption measurements at two different wavelengths over the ratio of the log of the wavelengths. The advantage of having optical property measurements conducted from the near-UV (355 nm) through the near-IR (700 nm) is the ability to start to separate out the influence of gas (such as $NO_2$) interferences on particle absorption and, more importantly, deconvolve the contributions of refractory black carbon and absorbing organic carbon or brown carbon (BrC) [*S Liu et al.*, 2015; *Saleh et al.*, 2013]. Analysis of BBOP biomass burning plumes provides evidence for primary brown carbon formation and brown carbon absorption changing as a function of downwind distance and

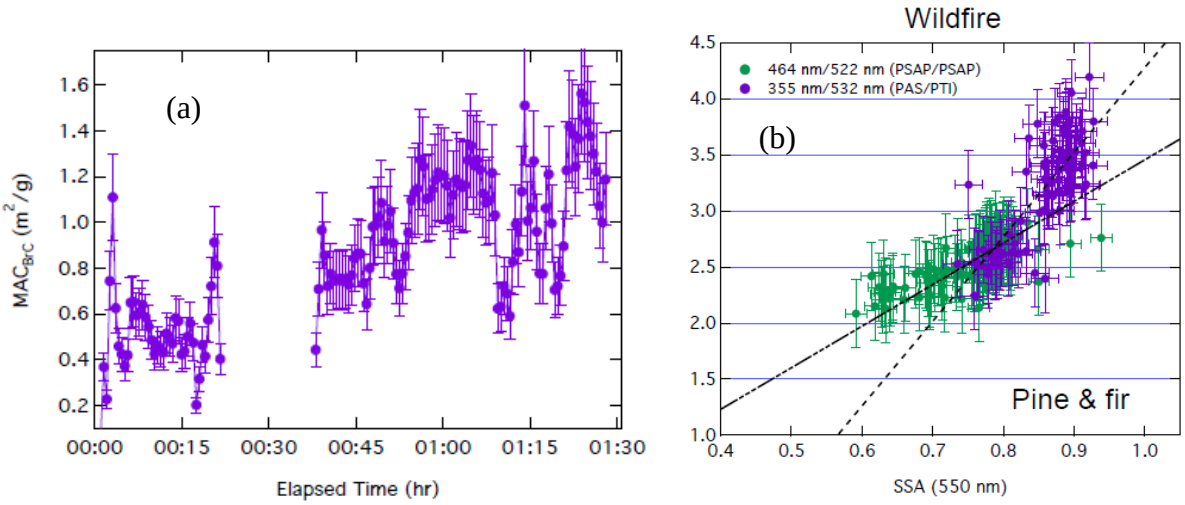


**Figure 7.** (a) Increase in measured 355 nm MAC as a function downwind from the Government Flats fire. (b) Relationship of the AAE (355 nm / 532 nm) to the SSA (550 nm) for wildland fires measured during BBOP.

atmospheric processing, suggesting secondary brown carbon formation. Figure 7a shows the increase in the measured 355 nm MAC downwind from the Government Flats fire on 21 August 2013. The increase in the 355 nm MAC suggests that secondary processes may be producing brown carbon absorbers in the plume during transport. Figure 7b shows the correlation between the measured AAE (355 nm / 532 nm) compared with the SSA (550 nm) for wildland fires. A manuscript on these results is in preparation [*Sedlacek et al.*, 2018b].

### 1.2 SP-AMS Data Analysis

The SP-AMS, developed by Aerodyne with DOE SBIR funding, uses laser-induced vaporization of black carbon-containing particles to detect and measure both the refractory black carbon (rBC) and the non-refractory components of ambient aerosol particles with a high resolution time-of-flight mass spectrometer [*Onasch et al.*, 2012]. The SP-AMS is the first instrument that makes in-situ, real-time, size-resolved chemical measurements of both the rBC and rBC-coating material and was deployed for the first time in an airborne campaign during BBOP. The ratio of the non-refractory to refractory particulate mass, $R_{BC}$ = [NR-PM]/[rBC], is related to photochemical aging and optical properties of rBC containing particles [*Cappa et al.*, 2012; *Massoli et al.*, 2012]. The SP-AMS also provides detailed mass spectral information about rBC structure (e.g., graphitic vs fullerenic) that can be used to identify rBC sources.

The BBOP study represents the first research flights for the SP-AMS instrument. The SP-AMS was operated during BBOP behind a constant pressure inlet and with both the laser and the resistively heated tungsten (standard AMS) vaporizers. The data acquisition included operating in mass spectra mode with 1 second time resolution and alternating the laser vaporizer ON and OFF. The laser OFF condition provides standard HR-AMS measurements that can be used for OA analysis and the laser ON condition provides rBC measurements.

The SP-AMS was operated with dual vaporizers for a large fraction of BBOP to enable chemical information on both the refractory black carbon (rBC) and nonrefractory particulate matter (NR-PM) to be measured. Figure 8b shows the average aerosol mass spectrum for the Colockum Tarps Fire plumes while Figure 8a shows the mass defects for the high-resolution peaks from the lower panel. The mass defect is the difference between the actual measured mass of a specific chemical ion and the nominal m/z at which the ion appears. This difference is a

function of the chemical formula of the ion with each additional hydrogen increasing the mass defect significantly, whereas carbon only ions have zero mass defects (by definition) and inorganics and metals typically having negative mass defects. Thus, the mass defect plot gives a quick visual overview of the particle chemistry. The colors in both plots represent the different chemical families listed in the legend. The average mass spectrum shown in Figure 8b was obtained with the dual vaporizer configuration and shows the relative magnitude differences between the measured rBC (in black) and NR-PM ion signals (colors). For almost all of the biomass burning plumes measured during BBOP, the ratio of the NR-PM-to-rBC ($R_{BC}$ = [NR-PM]/[rBC]) was large (i.e., >> 10). This observation is in direct contrast with recent urban [*Cappa et al.*, 2012] and rural [*S Liu et al.*, 2015] measurements where the $R_{BC}$ ratios were typically < 10, except for a few days with very high photochemistry. The final aspect to note from the average MS is that the biomass burning aerosol, even in the near-field (i.e., near the source), are oxidized (i.e., the average ratio of oxygen-to-carbon, O:C, is > 1 and the average oxidation state > -1). While these numbers register on the lower end of observed ambient oxidation levels [*Ng et al.*, 2011], these 'fresh' biomass burning emissions already show evidence of oxidation, either from the combustion or via atmospheric oxidation.

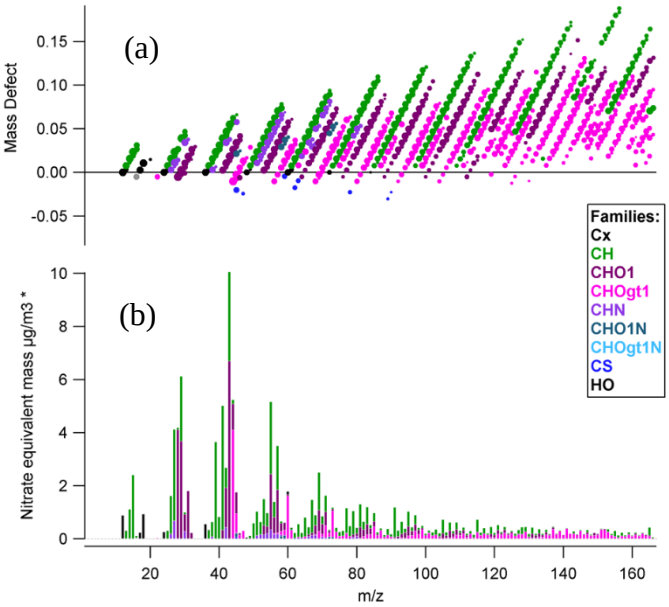


**Figure 8.** (a) Average particulate mass spectrum and (b) mass defect plot obtained for the Colockum Tarps Fire during the afternoon flight on 30 July 2013, showing relative chemical compositions of the ions.

*1.3.2 Refractory Black Carbon*

The refractory black carbon (rBC) mass loadings and, therefore, emission factors, were measured during BBOP using two different, but complementary techniques: (1) the Single Particle Soot Photometer (SP2) developed by Droplet Measurement Technologies (DMT) and (2) the SP-AMS.

The SP2 instrument measures the per-particle mass of rBC particles via a calibrated peak height measurement of the incandescence light emitted by laser-heated rBC particles inside the instrument. The SP2 is a single particle instrument, which provides the capability for high sensitivity to very low mass loading under typical ambient conditions, with limitations relating to only very small rBC particles [*Schwarz et al.*, 2010]. However, under very high particle number concentrations, such as may be found in near-field biomass burning plumes, the SP2 instrument can be affected by particle coincidence; that is, more than one particle can be sampled and detected at the same time, leading to an undercounting of the rBC particles and an underestimate of the total rBC particle mass. This issue has been well characterized over the years for optical particle counters, for example. The SP2 can be operated using a variable sample flow rate (with a constant particle free sheath flow) to change the sample dilution to ensure that coincidence does not occur; however, recent experiments designed to test the capabilities of the SP2,

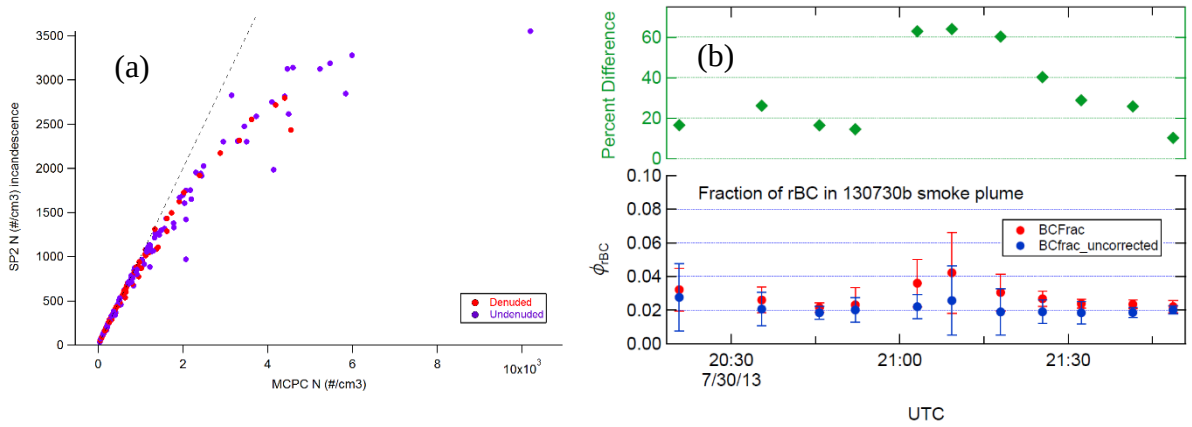


**Figure 9.** (a) SP2 particle counts vs mixing CPC particle counts for laboratory generated soot particles showing the effect of coincidence at high particle concentrations. (b) Uncorrected (red circles) and corrected (blue circles) SP2 data expressed as the mass fraction of rBC from the Colockum Tarps Fire. Green diamonds show the percent change upon correction.

conducted in our laboratories in collaboration with Drs. Sedlacek and Lewis, details potential issues with this approach [*Sedlacek et al.*, 2015].

For BBOP, SP2 coincidence was observed to be an issue when sampling some of the most concentrated biomass burning plumes. During a related laboratory project (DOE ASR funded BC4) held in our Boston College laboratories, we characterized the effects of coincidence on the same DOE ARM owned SP2 instrument used during BBOP. Further, in both the laboratory studies and BBOP, Dr. Sedlacek from BNL operated the SP2 using the same operational protocols. Figure 9a shows laboratory experiments detailing the effects of coincidence of well-characterized rBC particles on SP2 measurements by comparing with a well-calibrated mixing condensation particle counter (CPC) developed by Fred Brechtel (Brechtel Manufacturing). The laboratory results were used as a coincidence calibration and applied to the Colockum Tarps SP2 rBC particle counting data. Figure 9b shows the effects of applying the coincidence correction which can be as large as a 60% increase in the fraction of rBC.

The SP-AMS can provide chemical information on both the NR-PM and rBC particulate material when operated with dual vaporizers. The chemical information on rBC obtained by the SP-AMS is via carbon-only ion fragments ($C_n^+$) [*Onasch et al.*, 2015a; *Onasch et al.*, 2012]. Specifically, most rBC ion signals are measured in the $C_1^+$ to $C_5^+$ ions [*Corbin et al.*, 2014; *Onasch et al.*, 2015a]. However, as noted in section 1.3.1, the $R_{BC}$ ratio is very high for biomass burning particles. In the limit of very high $R_{BC}$, organic ion fragment contribution to the small $C_n^+$ ion signals can be large enough to cause interference. Figure 10a shows the ratio of $C_1^+$ to $C_3^+$ rBC ion signals as a function of the mass fraction of biomass burning particles sampled by an SP-AMS (with laser vaporizer only) during the 2009 EPA funded FLAME3 laboratory study. As highlighted in the beige box, rBC particles with rBC mass fractions greater than ~ 0.1exhibit $C_1^+/C_3^+$ ratios that agree very well with the ratio measured using the calibration carbon black particles (Regal black) [*Onasch et al.*, 2012]. For rBC mass fractions below 0.1, the $C_1^+/C_3^+$ ratio increases dramatically due to $C_1^+$ ion fragments from the high organic mass loadings. In fact, Figure 10b shows the $C_n^+$ ion signal generated from organic ion fragmentation when

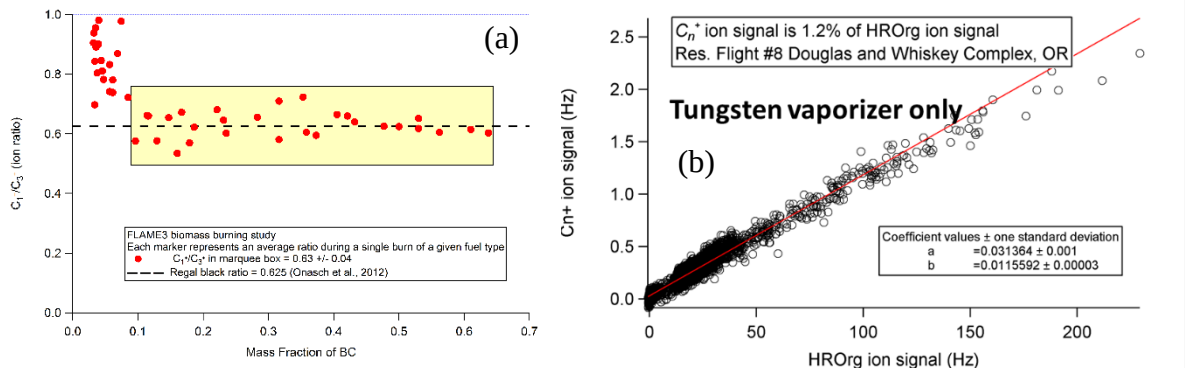


**Figure 10.** (a) C1+/C3+ carbon cluster ion ratio for biomass burning samples measured during the 2009 FLAME3 laboratory study. (b) The Cn+ ion signal measured during the Douglas and Whiskey Complex fire generated from the tungsten vaporizer only.

sampling the Douglas Whiskey Complex, OR during BBOP using the SP-AMS operated with the tungsten vaporizer only (i.e., laser vaporizer was off). The high [Org] generates $C_n^+$ ion signals (~1.2% of total organic ion signal) that interfere with rBC $C_n^+$ ion signals.

During BBOP, the high organic mass loadings generated $C_n^+$ ion signals that were approximately equal to the measured $C_n^+$ ion signals from rBC particle types. While this $C_n^+$ ion interference was observed to be significant, the fragmentation patterns of the two different contributions to the $C_n^+$ ion signals from rBC and Org species are significantly different. This difference in the fragmentation patterns provides a direct method for separating ions measured from these two sources. Figure 11 shows the differences in the $C_n^+$ ion fragmentation. Figure 11a shows the measured $C_n^+$ ion fragmentation pattern with laser vaporizer only (and dual vaporizers) for the calibration material (Regal carbon black) (top panel), the average fragmentation pattern from sampling of biomass burning plumes from the Douglas and Whiskey Complex, OR using the SP-AMS with tungsten vaporizer only (middle panel), and the average fragmentation pattern from the Colockum Tarps fire using the SP-AMS with dual vaporizers.

We can use factorization methods for deconvolving the apportionment of the $C_n^+$ ion signals into the rBC and Org components. Figure 11b shows the results from running Positive Matrix Factorization (PMF) on the $C_n^+$ ion signals from the Government Flats fire (21 August 2013). The PMF factors were selected based on two criteria: (1) normal PMF parameters indicating solution acceptability and (2) the empirical goal of obtaining an rBC factor that returns a $C_1^+/C_3^+$ ion signal ~0.625, as consistently measured for our calibration particles (Regal carbon black) and observed for almost all biomass burns sampled during the 2009 FLAME3 project (Figure 10a). The PMF results in Figures 11b and 12 show that we were able to meet both criteria reasonably well. Figure 12 shows the results of applying the PMF determined apportionment of the $C_n^+$ ions into rBC and Org components for two plume transects during the Government Flats fire, sampled on 21 August 2013, where during the first transect (left) the SP-AMS was operated with dual vaporizers and during the second transect (right) the SP-AMS was operated with the tungsten vaporizer only. When the SP-AMS was operated with dual vaporizers, the $C_n^+$ ion signal is deconvolved to show a ~50% split between rBC and Org contributions. When the SP-AMS is operated with the tungsten vaporizer only, the $C_n^+$ ion signal is shown to be almost 100% composed of the Org component, as it should. These results show that we can separate out the rBC and Org contributions to the measured $C_n^+$ ion signals.

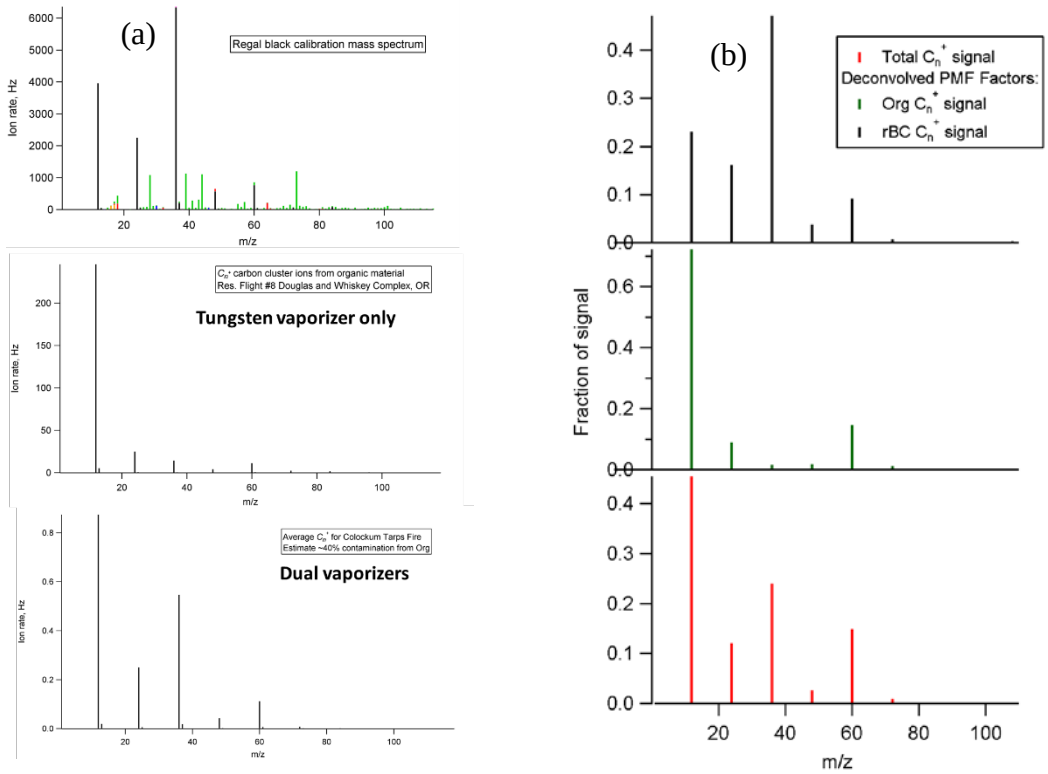


**Figure 11.** $C_n^+$ ion fragmentation patterns for (a) calibrant (Regal carbon black) using the SP-AMS laser vaporizer (top), biomass burning organic aerosol sampled during BBOP with the tungsten vaporizer only (middle), and biomass burning aerosol sampled during BBOP with dual vaporizers (bottom). The $C_n^+$ ion fragmentation patterns shown in (b) correspond to average Cn+ ion signal measured during the Governmental Flats fire (bottom) and the PMF-derived Organic component (middle) and rBC component (top).

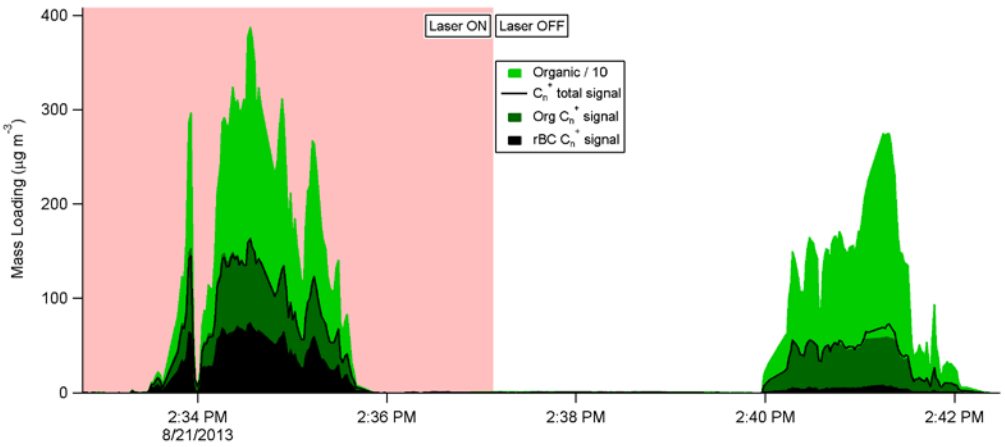


**Figure 12.** Two plume transects during the Government Flats fire, sampled on 21 August 2013, where during the first transect (left) the SP-AMS was operated with dual vaporizers and during the second transect (right) the SP-AMS was operated with the tungsten vaporizer only.

*1.3.3 Non-refractory Chemical Composition*

The primary measurement of NR-PM chemical composition comes from the SP-AMS. Data analysis has been conducted to identify and fit all of the high-resolution mass spectral peaks in the 1 second mass spectra. An example average mass spectrum from the Colockum Tarps fire is shown in Figure 8b colored by chemical families. The total organic aerosol loadings and several organic markers are shown in Figures 13 and 14 as a function of downwind transport distance for this same fire. Figure 13 shows the ratio of the change in organic to the change in CO in the plume relative to background (outside the plume) as a function of downwind distance. The increase in organic is higher for the more smoldering part of the fire (purple points), but relatively constant with downwind distance, possibly due to a balance between evaporation of primary organic aerosol and condensation of secondary organic aerosol.

One of the key climate-relevant objectives of the project is understanding the balance between evaporation rates of primary organic aerosol (POA) upon dilution and the production rates of both secondary organic aerosol (SOA via functionalization) and smaller VOCs from biomass burning SVOC precursors via fragmentation. In particular, the goal is to understand why some biomass burning events form large amounts of SOA (SOA/POA > 1), which has been observed consistently in laboratory experiments [*Hennigan et al.*, 2011], whereas in some field observations the ORG/CO has been observed to be relatively constant downwind (similar to Figure 13) [*Cubison et al.*, 2011] while other field observations suggest that the emitted ORG concentration can be explained by dilution alone [*May et al.*, 2015].

We observe nearly constant ΔORG/ΔCO ratios in the near-field a few hours downwind from the combustion source, while we also observe consistent evidence of photochemical oxidation occurring during the downwind transport. These observations come from gas phase measurements [*Kleinman and Sedlacek*, 2016] and from the chemical signatures from the SP-AMS mass spectra. These observations support the concept that primary organic material is vaporizing/reacting, decreasing the organic mass loading at the same time that secondary organic material is condensing from the gas phase in a dynamic quasi-equilibrium. Figure 14 shows the ratio of signal at m/z 60 ($C_2H_4O_2^+$ ion, associated with levoglucosan, a marker for biomass burning) to total organics (f60) and the ratio of oxygen to carbon (O:C), both measures of the chemical composition of BBOA. The f60 is higher for the more smoldering part of the fire (purple points) consistent with higher emissions of anhydrous sugars during inefficient

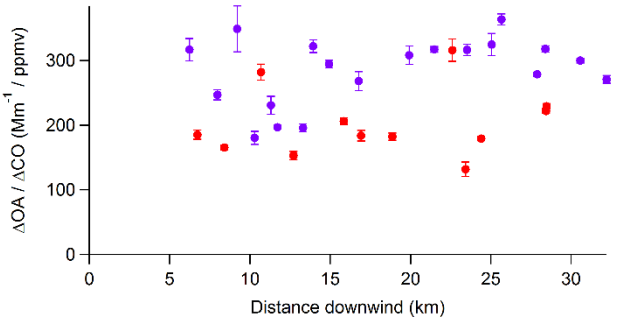


**Figure 13.** Ratio of change in organic to change in CO for the Colockum Tarps Fire. Red and blue symbols indicate two different parts of the plume.

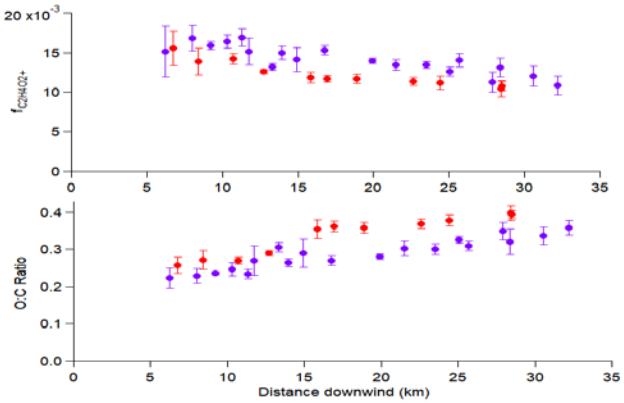


**Figure 14.** Ratio of signal at mz 60 to total organics and O:C ratio as a function of downwind distance for the Colockum Tarps Fire.

combustion. The O:C is lower for the more smoldering conditions, consistent with less chemical processing of the flame emissions. In contrast to the trend in total organics with downwind distance, both f60 and O:C show significant changes. Decreasing f60 with aging of BBOA has been observed previously, as has increasing O:C as the organic aerosol undergoes photochemical processing [*Cubison et al.*, 2011; *Hecobian et al.*, 2011].

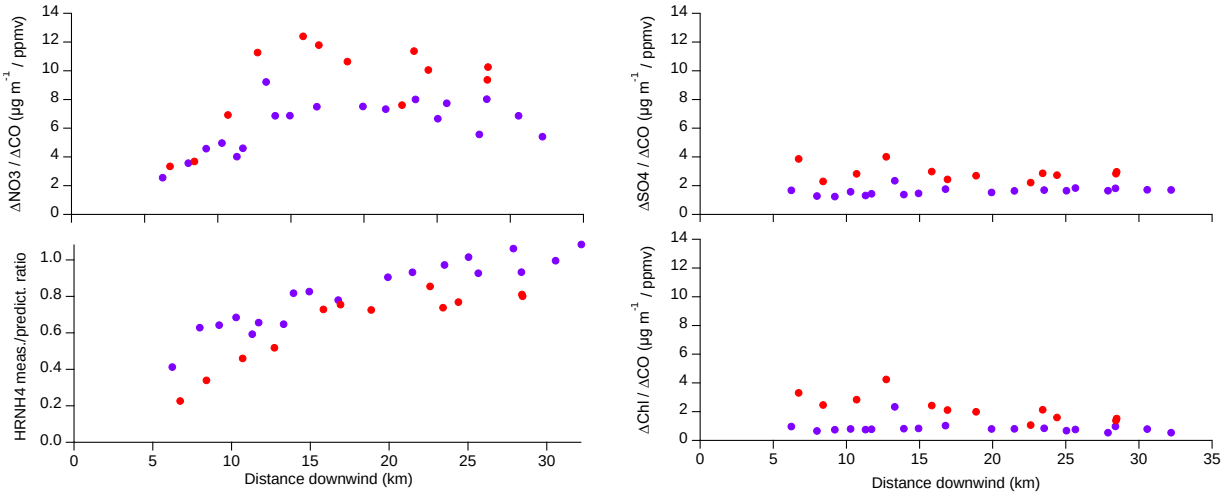


**Figure 15.** Ratio of change in $NO_3$, $SO_4$, $NH_4$ and Chl to change in CO for the Colockum Tarps Fire. Red and blue symbols indicate two different parts of the plume.

In addition to organic chemical composition, the SP-AMS also measures the non-refractory inorganic composition (i.e., $NO_3$, $SO_4$, $NH_4$, and Chl). While these inorganic species are typically observed to be in much lower concentrations than the overall organic loadings, they also provide useful insights into processes that are occurring in the plume as a function of fuel type, combustion conditions, and downwind atmospheric processing. For example, during the Government Flats fire on 21 August 2013, the SP-AMS measured what appears to be primary SO4 mass being emitted from the fire while simultaneously measuring what is mainly secondary NO3 formation. Figure 15 shows the trends for the Colockum Tarps Fire of the measured change in $NO_3$, $SO_4$, $NH_4$, and Chl relative to change in CO as a function of distance downwind. $\Delta SO_4/\Delta CO$ is relatively constant, suggesting that $SO_4$ is a primary emission. In contrast, the measured $\Delta NO_3/\Delta CO$ increased significantly with distance from the fire, indicating potential particulate nitrate formation. For these measurements, the SP-AMS seems to be measuring the nitrate mainly in the ammonium nitrate salt form, whereas the $SO_4$ is likely a potassium or sodium salt. However, the interesting aspect of this data is to assess how much of the secondary brown carbon might be related to organic nitrate formation. Organic nitrates are known to absorb in the near-UV (i.e, ~355 nm) and may be responsible for the observed increase in the measured MAC at 355 nm (Figure 7). This combined optical and chemical analysis is being prepared as a manuscript [*Sedlacek et al.*, 2018b]

### 1.3 Comparison of G-1 and Mount Bachelor Observatory Measurements

We compared measurements from the G-1 with measurements at Mt. Bachelor Observatory made with a high-resolution time-of-flight aerosol mass spectrometer (HR-AMS) operated with Professor Qi Zhang and her group [*Collier et al.*, 2016]. Figure 16a shows a map of these measurements. These measurements represent a detailed look at the regional influence of the biomass burning occurring in the Pacific North West. The characteristics of the measured

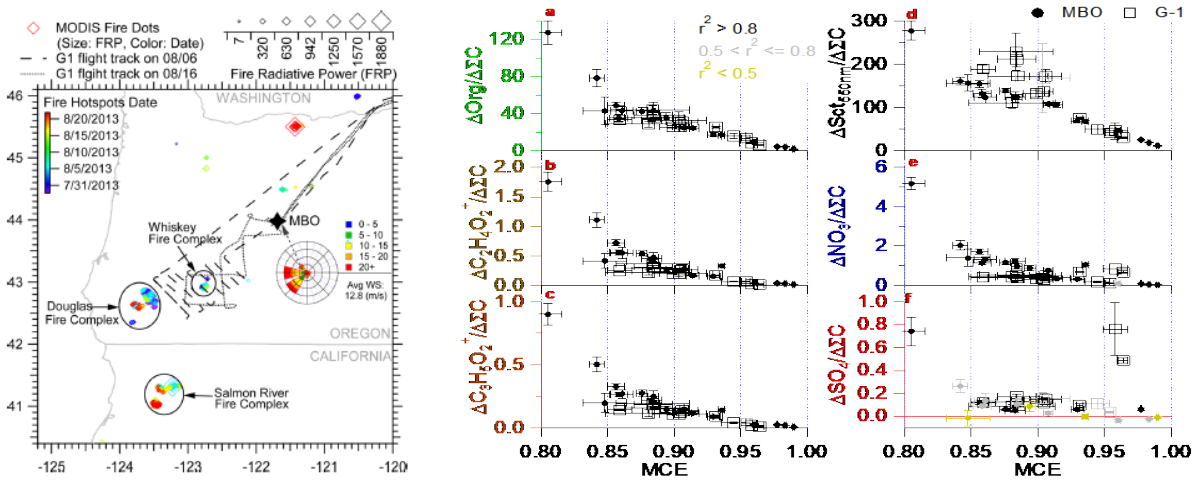


**Figure 16.** (a) Map of MBO and the G-1 coordinated flight paths. (b) Measured particulate organic, light scattering, NO3, and SO4 to the sum of CO+CO2 as a function of the burn MCE.

aerosol emissions were found to depend strongly on the modified combustion efficiency (MCE), a qualitative index of the combustion processes of a fire.

The G-1 flew three research flights over MBO during BBOP and sampled the same smoke plumes that drifted over MBO, spanning atmospheric residence times from ~ 1 to 45 hours, enabling a comparison of the biomass burning organic aerosol measured by the HR-AMS at MBO and the G-1 SP-AMS operated with only the tungsten vaporizer. Figure 16b shows that MCE appears to be one of the dominant variables to determine the measured downwind (i.e., regional) particulate organic, $NO_3$, $SO_4$, and scattering relative to the sum of [CO] plus [CO2]. These results suggest that on a regional scale, some of the particulate properties may be potentially modeled using a simple MCE-dependent parameterization.

The measured organic aerosol chemistry appears to be more dependent upon the atmospheric residence time than the overall ORG/(CO+CO2) loadings. Figure 17 shows the results for $f6_{C2H4O2}$ (i.e., f60), H:C, O:C and carbon oxidation state ($OS_C$) for 32 plumes as a function of MCE. The solid circles show the 18 plumes measured at MBO and the open squares show the 14 plumes measured on the G-1. The colors indicate the plume transport time at MBO as determined from HYSPLIT back-trajectories.

The strong decrease in f60 with MCE suggests that both flaming conditions and plume aging contribute to decreasing f60, and that caution should be exercised when using f60 as an indicator of plume age. Similarly, O:C increases and H:C decreases with both MCE and plume age. OSc ( = 2 × O:C – H:C), considered a more reliable metric for the average oxidation state of organic aerosol [*Kroll et al.*, 2011], also increases with both MCE and plume age (compare the relatively young G-1 open squares with the older MBO solid circles). Thus, the flaming conditions of wildfires, in addition to plume age, need to be considered when assessing the impact of BBOA on regional climate models.

### 1.4 Emission Factors

Professor Yokelson led a team of scientists that calculated emission factors (EF, g/kg of dry fuel burned) for the gas-phase and particle-phase emissions from some of the BBOP sampled fires to improve air quality models. Phase one was a detailed assessment of the available data with the assistance of UM graduate student Vanessa Selimovic, combined with examination of flight tracks and HYSPLIT back-trajectories. Due to frequent removal of the PTR-MS from the

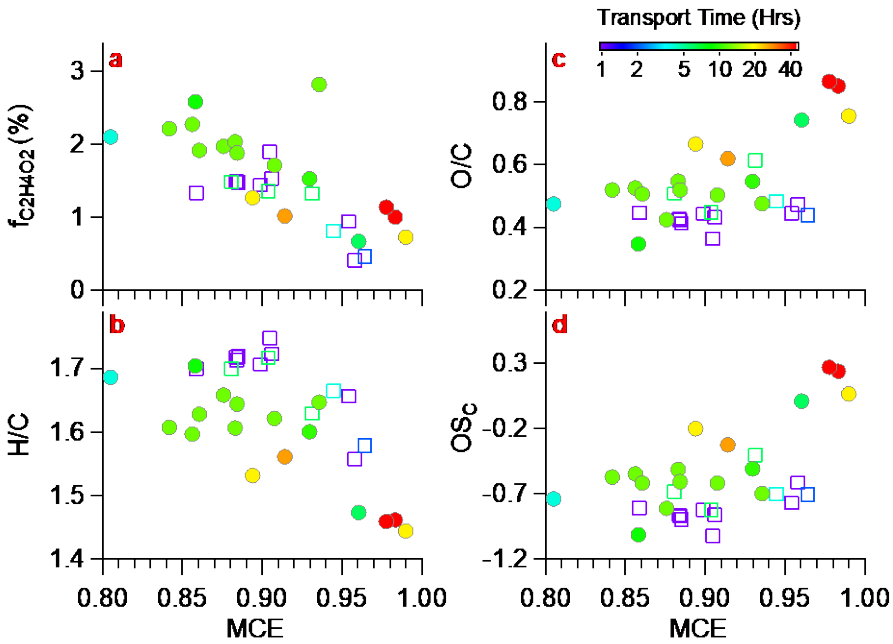


**Figure 17**: The parameters depicted here are calculated for each of the 32 plumes where solid circles are for MBO and open squares are for G-1. They include (a) the fractional contribution of $C_2H_4O_2^+$ to the total signal, (b) H/C, (c) O/C, and (d) $OS_C$ vs MCE. All data points are colored by approximate transport time.

G-1, only one wildfire from BBOP (Colockum Tarps Fire in central Washington) had detailed non-methane organic gas (NMOG) data, but this was a critical fire as it expanded the range of ecosystems studied to the much drier interior west and included herbaceous (grass) fuels. Furthermore, the Colockum Tarps Fire was fortuitously sampled by the G-1on one of its largest growth days giving insight into the type of fire behavior responsible for much of the total smoke production. On the day of G-1 sampling, the fire had grown from 14,000 hectares 3 days earlier to 24,000 hectares. Fuels burned were mainly timber, brush and grass. Four fresh plumes, less than 20 min old, were used for the emission ratio analysis. Fuel consumption data suggests that total emissions from this fire could exceed one Tg, on a par with total fossil fuel emissions from a large state or small country.

In the process of analyzing the G-1 data we noted that m/z 87 for the PTR-MS was incorrectly labeled as a biogenic emission. Our previous work with high-resolution MS in smoke unambiguously shows this peak is actually butanedione and our modeling work has identified this as a key precursor for PAN and thus also subsequent ozone formation downwind [*Müller et al.*, 2016]. The results for this fire were combined with two other fires observed from the DC-8 during the Studies of Emissions and Atmospheric Composition, Clouds and Climate Coupling by Regional Surveys (SEAC4RS) campaign to yield emission factors (EF, ratio to fuel burned) and emission ratios (ER, ratio to change in $CO_2$ + CO).

Table 3, reproduced from Liu et al. [2017], compares the results with measurements from prescribed burns and from the MBO measurements. In all cases, organic aerosol represented the majority (> 90%) of the mass emitted, and the EF for the Western wildfires analyzed in this work are 2 to 5 times larger than those for prescribed burns. This same trend holds for the dominant inorganic species. The measured EFs were used to estimate annual emissions from wildfires in the Western US for comparison with the 2011 national Emissions Inventory (NEI). While gas-

**Table 3. Reproduced from Liu et al. [2017]**

**Table 4.** Comparison of Aerosol EFs (g $kg^{-1}$) and ERs to $\Delta(CO_2 + CO)$ for Temperate Fuels Measured From Aircraft

| Fire | Western Wildfires (This Work) | | Prescribed Chaparral Fires [*May et al.*, 2014] | Prescribed Montane Fires [*May et al.*, 2014] | Prescribed SE Coastal Plain Fires [*May et al.*, 2014] | Western Wildfires [*Collier et al.*, 2016] |
|---|---|---|---|---|---|---|
| MCE | 0.912 (0.031) | | 0.924 (0.019) | 0.899 (0.020) | 0.936 (0.014) | 0.91 (0.046) |
| | EF (g $kg^{-1}$) | ER to $\Delta(CO_2 + CO)$ ($\mu g\ m^{-3}\ ppm^{-1}$) | EF (g $kg^{-1}$) | EF (g $kg^{-1}$) | EF (g $kg^{-1}$) | ER to $\Delta(CO_2 + CO)$ ($\mu g\ m^{-3}\ ppm^{-1}$) |
| OA | 24.3 (6.1) | 30.0 (8.1) | 3.9 (1.8) | 11.2 (2.7) | 2.8 (1.6) | 31 (24) |
| BC | - | - | 1.43 (0.13) | 0.59 (0.13) | 1.11 (0.67) | - |
| $NH_4$ | 0.34 (0.15) | 0.42 (0.19) | 0.05 (0.05) | 0.06 (0.00) | 0.07 (0.03) | 0.32 (0.32) |
| $NO_3$ | 0.87 (0.13) | 1.08 (0.18) | 0.08 (0.07) | 0.20 (0.00) | 0.09 (0.03) | 0.81 (0.94) |
| Chl | 0.19 (0.20) | 0.23 (0.24) | 0.08 (0.05) | 0.01 (0.00) | 0.09 (0.15) | - |
| $SO_4$ | 0.30 (0.16) | 0.37 (0.18) | 0.01 (0.01) | 0.01 (0.00) | 0.17 (0.10) | - |
| $PM_1$ | 26.0 (6.2) | 32.1 (8.2) | 5.5 (1.7) | 12.1 (2.9) | 4.4 (2.0) | - |

phase emissions were generally comparable between these measurements and the NEI, our PM emission estimate was more than a factor of 3 larger than the NEI. This suggests that particulate emissions from biomass burning in the Western US may be significantly underestimated.

### 1.5 Analysis of TEM Grids

Aerosol particles were collected onto TEM grids (lacey carbon substrates) using a two-stage impactor sampler throughout all of the research flights of the G-1. These grids were analyzed to determine the population and intra-particle (morphology) mixing states of the biomass burning particles. The mixing state of the refractory black carbon particles, in

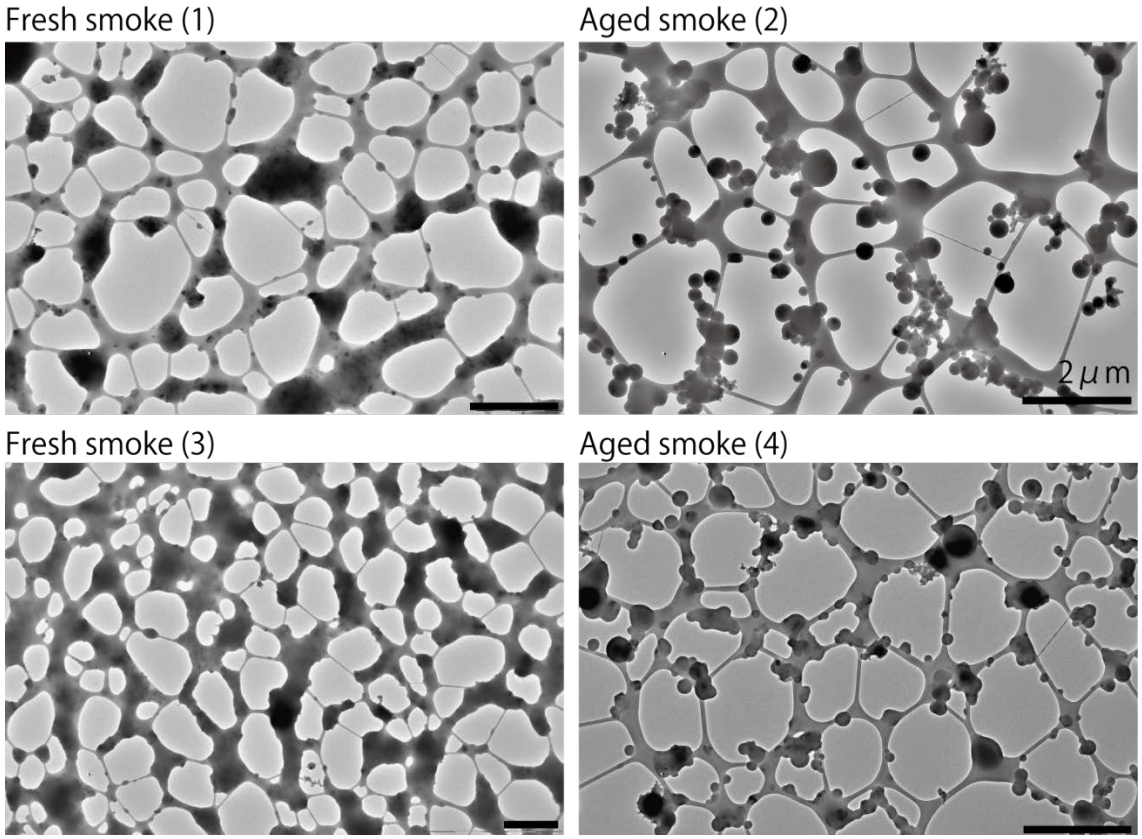


**Figure 18.** TEM images of aerosol samples from biomass burning during the BBOP 2013 0730b flight.

particular, may play a significant role in the optical properties (i.e., absorption and SSA) of the biomass burning smoke [*Onasch et al.*, 2018]. In addition to investigating the mixing state of the biomass burning particles, the TEM images are the only current method that can identify tar balls.

Tar balls (TBs) are spherical, highly viscous, organic aerosol particles that have been observed to be emitted or form in biomass burning [*Pósfai et al.*, 2004]. Tar balls may be absorbing (i.e., brown carbon) and may have different climate impacts than other types of carbonaceous particles [*Chakrabarty et al.*, 2010; *Feng et al.*, 2013]. Tar balls display no deformation on the filters, suggesting they were solid or highly viscous when collected. Dr. Buseck and Dr. Adachi obtained TEM images for all the samples to measure the TB number fractions, which were measured visually from representative images (e.g., Figure 18). There were almost no TBs in fresh smokes, which however contained liquid aerosol particles (Figure 19, panels 1 and 3). In contrast, many TBs occurred in the aged biomass burning smoke (~2.5h from emission, Figure 19, panels 2 and 4). Similar TB formation was also observed in other wild fires during the BBOP campaign, whereas there were almost no TBs in agricultural smokes collected during the campaign. An analysis of samples from 11 BBOP flights showed that the tar ball number fraction was near 0 at or close to the flame, and increased to 30 to 80% downwind. This analysis of tar ball formation as a function of plume age suggests that tar balls are processed primary particles, rather than being directly emitted from fires.

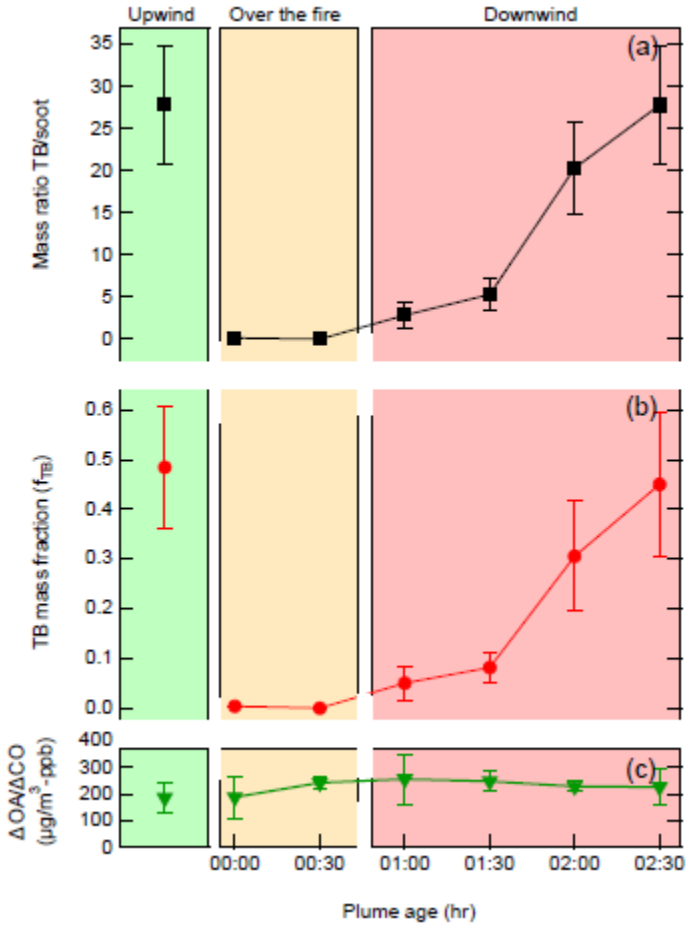


**Figure 19.** (a) Mass ratio of tar balls to soot, (b) Mass fraction of tar balls in the total organic mass loading, and (c) ratio of organic to CO to account for dilution as a function of plume age in the Colockum Tarps Fire.

A more detailed analysis of the Colockum Tarps Fire combined the measurements from the TEM images (number and mass), SP-AMS (organic mass loadings), and SP2 (refractory black carbon mass loadings) to give a first ever estimate of the mass fraction of tar balls in the organic aerosol emissions from wildfires [*Sedlacek et al.*, 2018a]. This calculation assumes that the TEM-derived soot loadings are the same as the SP2 rBC mass loadings and that the SP-AMS can detect tar balls. Figure 19b shows the estimated tar ball mass fraction of the total organic mass loadings as a function of biomass burning plume age during the Colockum Tarps Fire 30

July 2013. Figure 19c shows that the increasing mass fraction of tar balls was not accompained by an increase in total organic loading, making formation by gas-to-particle condensation implausible. This suggests that tar balls are processed primary particles. In addition, the signifcant mass fraction suggests that tar balls need to be considered in emissions inventories since they have different optical properites than organic aerosol.

**Task 2. Small Scale Laboratory Experiment: Tar Balls (Year 2)**

In this task, our goals were to (a) characterize the physiochemical properties of laboratory-generated tar balls from BBOP-related fuel materials, (b) characterize and quantify BBOP measurements of tar balls by the SP2 (Dr. Sedlacek, BNL), SP-AMS (ARI), and optical instrumentation (BNL and ARI) with and without thermal denuding, and (c) compare laboratory results as a function of fuel type with field observations to investigate potential variations in formation, chemical compositions, phase, and particle volatilities. Specific issues of interest include (a) identifying whether tar balls contain refractory black carbon, (b) assessing the collection efficiencies of tar balls impacting on the 600$^{o}$C heated tungsten vaporizer in the AMS (i.e., given the observed low volatilities might AMS measurements be underestimating organic biomass burning plume loadings), (c) measuring the wavelength-dependent, mass-specific absorption cross-sections of brown carbon components, and (d) measuring the chemical composition of tar balls to provide insights into the atmospheric processes that form (evaporation/oxidation) and modify tar balls in biomass burning plumes as a function of transport time.

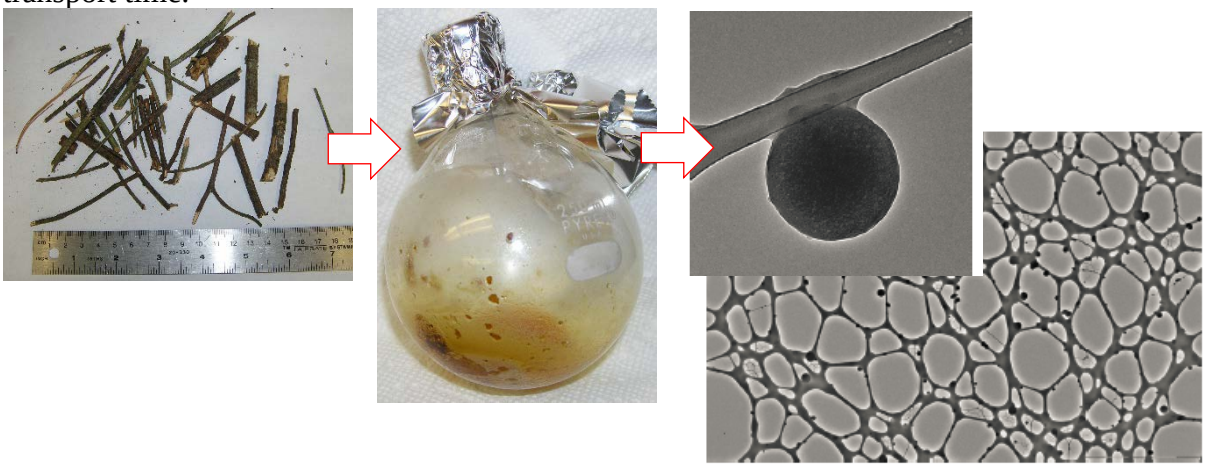

**Figure 20.** Pine needles and twigs were pyrolyzed at 500 to 600 C under air or N2. TEM grids showed the presence of low-volatility, spherical particles in 8 out of the 22 experiments.

We built an experimental apparatus similar to that detailed by Toth et al. [2014], in which liquid tars prepared from representative biomass fuels are emulsified in water, aerosolized by bubbling nitrogen through the tar-water emulsion, then rapidly heated to 600$^{o}$C to produce the tar balls. We generated the tar by pyrolyzing pine twigs, needles and duff in a round bottom flask held in a heating mantle at 500 to 600 C. Vapors were collected in a condensing flask held in an ice bath. The condensate was a pale-yellow liquid. We also observed viscous black tar dripping into the collector flask. For most experiments, the pyrolysis was conducted in air, but for some we used a pure N2 carrier gas. The condensate was dissolved in methanol for most experiments.

For a few, we dissolved the condensate in water. Particles were generated from the dissolved condensate either using a plastic tube suspended above an ultrasonic nebulizer (Exo Terra Fogger PT2084) or using a single jet BGI nebulizer. The particles were dried in a diffusion dryer (if water was the solvent) or a charcoal diffusion dryer (if methanol was the solvent) and passed through a tube furnace at 600 C. The carrier gas flow through the tube furnace was 2 lpm. Immediately upon exiting the tube furnace, the flow was diluted with 10 lpm of clean dry air to reduce homogenous nucleation of gas-phase organics. The particles were passed through a 2.5 μm cut cyclone and two 2 L reservoirs. Further dilution was required to keep the particle loading from overwhelming the SP-AMS and SP2. We diluted by a factor of 5 to 10 with a home-built loop diluter, and a further factor of 10 to 100 with a filter diluter.

The particles were sampled continuously by the SP-AMS, the SP2 and an SMPS. Periodically, samples were collected on lacey and formvar TEM grids for analysis to determine the number of tar balls by ASU. We collected 22 TEM samples and 8 of them showed a significant number of high-viscosity, low-volatility spherical particles that we interpreted to be tar balls. Figure 21 compares the SP-AMS mass distribution (tungsten vaporizer only) with the SMPS volume distribution for one of the experiments in which the TEM grid showed predominantly tar balls. This comparison gives an estimated density of 1.6 g/m$^3$, in reasonable agreement with the literature value of 1.5 g/cm$^3$. Converting the SMPS volume distribution to a mass distribution and comparing to the SP-AMS mass distribution suggests that the collection efficiency in the SP-AMS for laboratory generated tar balls is approximately 1. This further suggests that tar balls present in the wildfire plumes during BBOP, if they are similar to laboratory generated tar balls, should have been detected with the SP-AMS.

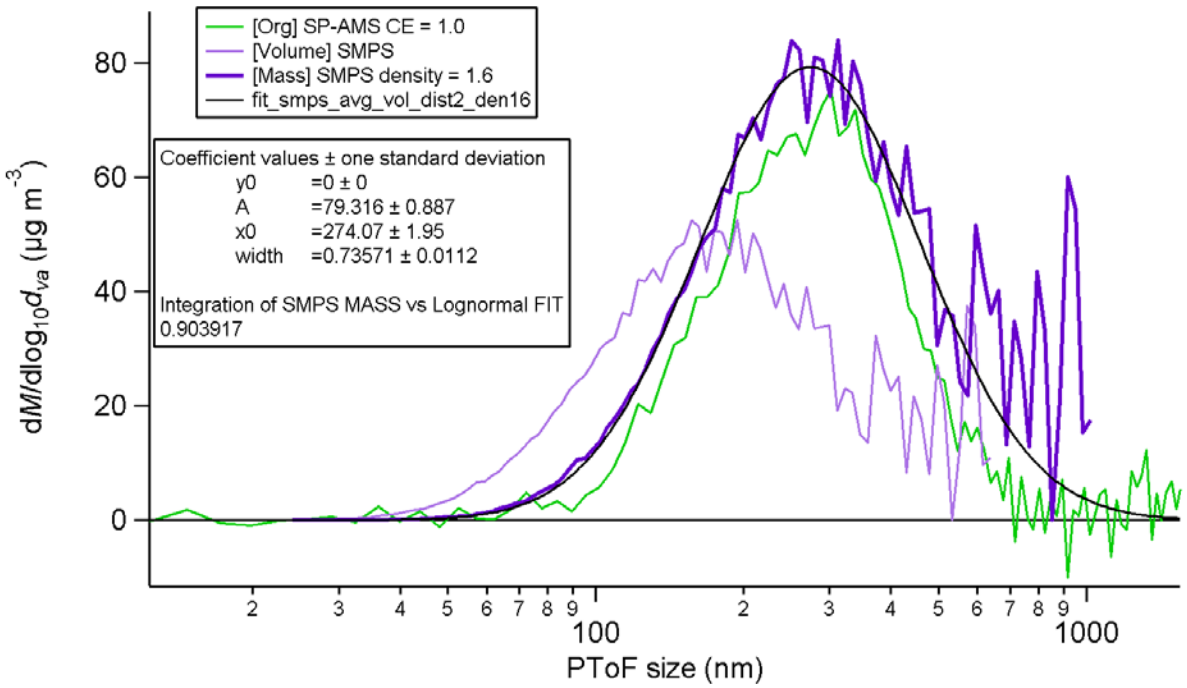


**Figure 21.** Comparison of the SP-AMS mass distribution (green line) with the SMPS volume distribution (thin purple line) gives a density of 1.6 g/m$^3$. Converting the SMPS volume distribution to a mass distribution with this density and comapring to the SP-AMS mass gives an estimated collection efficiency of ~ 1 for tar balls in the SP-AMS.

The high-resolution mass spectrum of laboratory generated tar balls shows prominent peaks at high m/z due to large unsaturated hydrocarbons which may be aromatic in nature and contribute to brown carbon absorption (Figure 22). In contrast, the mass spectra collected during BBOP do not show these particular peaks. Positive matrix factorization (PMF) analysis of the Colockum Tarps Fire resulted in a series of increasingly oxidized factors that increased as a function of plume age. However, the most aged factors, which should represent wildfire tar balls based on timing, do not match the mass spectrum of the laboratory generated tar balls. This suggests that the laboratory generated tar balls may have a different chemical composition than wildfire generated tar balls.

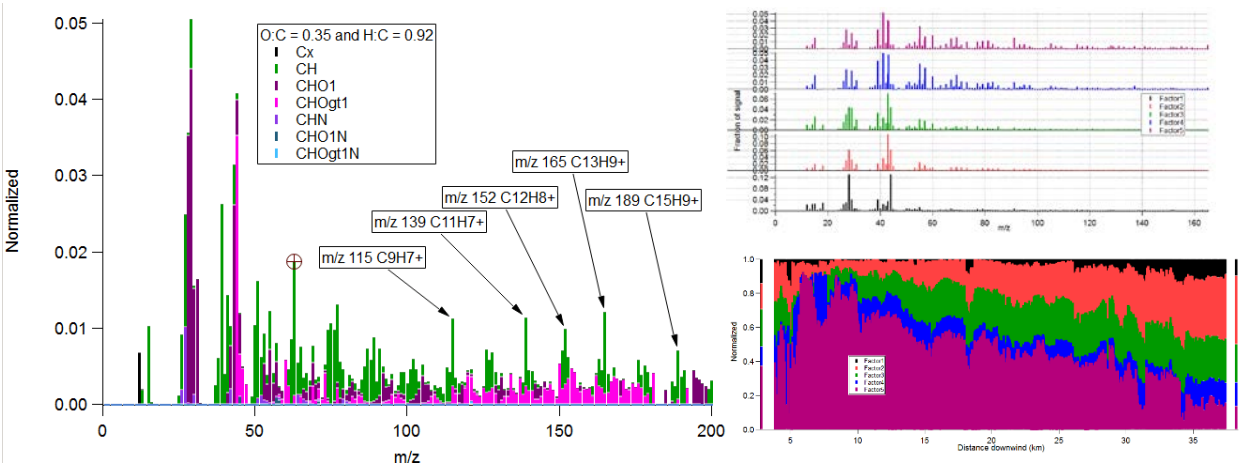


**Figure 22.** (Left) High-resolution mass spectrum of laboratory generated tar balls. (Right) PMF analysis of organics measured downwind of the Colockum Tarps Fire showing increasing oxidation with plume age.

Interestingly, the SP2 measured rBC signals from the tar balls. Since tar balls are expected to consist of predominantly BrC with little or no BC, this result suggests that some charring of tar balls may occur during SP2 detection. This result was confirmed in later laboratory measurements of nigrosin particles, a light absorbing dye, that showed significant charring in the SP2 [*Sedlacek et al.*, 2018c]. This suggests that measurements of rBC with the SP2 in wildfire plumes may be over-estimated.

We intended to repeat this laboratory tar ball generation experiment in Year 3 of the project. However, analysis of the BBOP TEM grids showed that in wildfire plumes, the tar balls are produced with aging of the plume. This is different than the mechanism proposed by Toth et al. [2014], and emulated in the laboratory experiments, in which tar balls are formed by heat shock of tar droplets in the flame front. Since there are also optical and chemical differences between wildfire and laboratory generated tar balls, it is not clear how closely laboratory generated tar balls represent those measured in the field. We decided to defer further laboratory experiments until we have a better experimental setup for generating tar balls that mimics how they form in wildfires.

During Year 3, we instead conducted a series of laboratory experiments to better characterize SP-AMS detection. The SP-AMS can operate with one of two particle vaporizers: (1) the standard AMS resistively heated tungsten vaporizer for traditional detection of non-refractory particulate matter (NR-PM), and (2) an intracavity laser vaporizer for detection of absorbing, refractory materials, including black carbon (rBC) and metal nanoparticles, and associated NR-PM. The SP-AMS can also be operated with both vaporizers simultaneously, by

sequentially turning the laser vaporizer on and off over the course of sampling. While each vaporizer has been shown to be effective when operated separately, the use of both simultaneously is complicated by the different collection efficiencies (CE) of the two vaporizers and can strongly affect the measured NR-PM signals from both rBC-containing and non-rBC-containing particles.

Figure 12 shows a comparison of organic mass loading in the two different detection modes from the Government Flats Fire during BBOP, and Figure 23 shows the increase in mass loading when turning on the laser vaporizer for typical ambient data during the DOE funded campaign in Detling, UK in 2012. Nominally, the only difference should be the detection of any refractory (i.e., BC) components in the particles. Figure 23 shows that all non-refractory aerosol components are greater during laser on, even for species not expected to be internally mixed with rBC (e.g., nitrate). This effect appears to be due to laser heating of the ionization chamber. As shown in Figure 24, turning the laser on increases the temperature of the vaporizer by 10 degrees, but increases the temperature of the ionization chamber by 90 degrees. Increasing the temperature of the ionization chamber can in turn increase detection of the particles that bounce off the tungsten vaporizer and impact the ionization chamber.

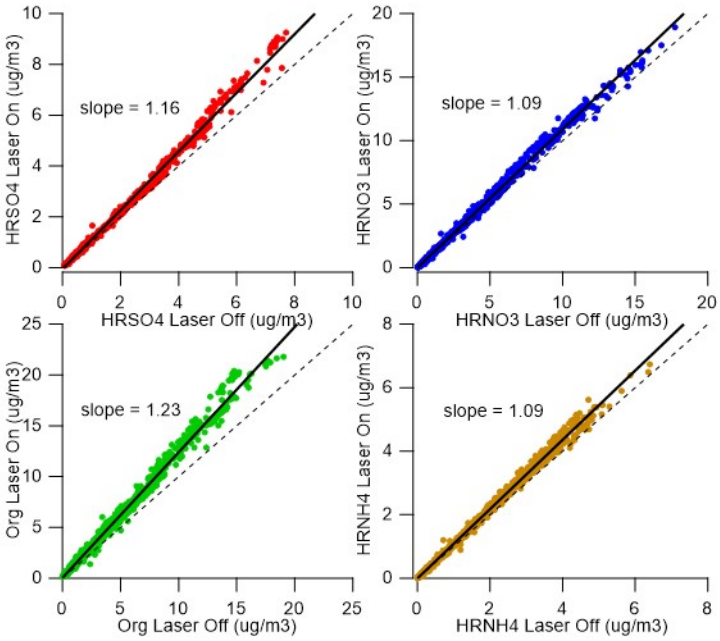


**Figure 23**. AMS mass loading measured with both vaporizers (laser on) vs measured with tungsten vaporizer only (laser off) from the DOE funded campaign in Detling, UK in 2012.

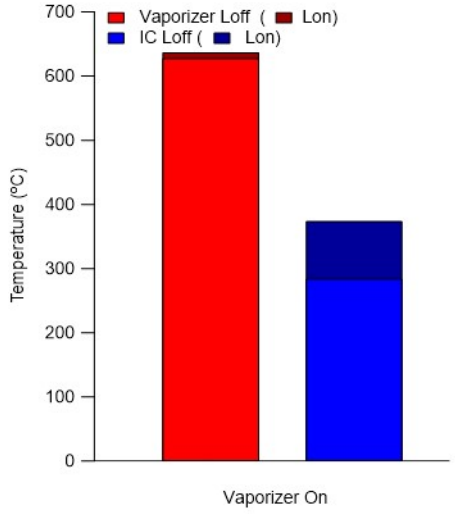


**Figure 24**. Temperature of the vaporizer (red) and ionization chamber (blue) with laser off and laser on.

In order to analyze the effect of the laser on the temperature of the vaporizer and ion chamber, as well as constrain potential laser positions, a series of experiments were conducted with baffles installed in 3 distinct locations in the detection region of the AMS, (1) attached to the filament holder, (2) between the Nd:YAG crystal and the coupling flange, and (3) on a mounting piece approximately equidistant between the two. Several sizes (diameters) were used, and baffles were added both individually and in combination with each other.

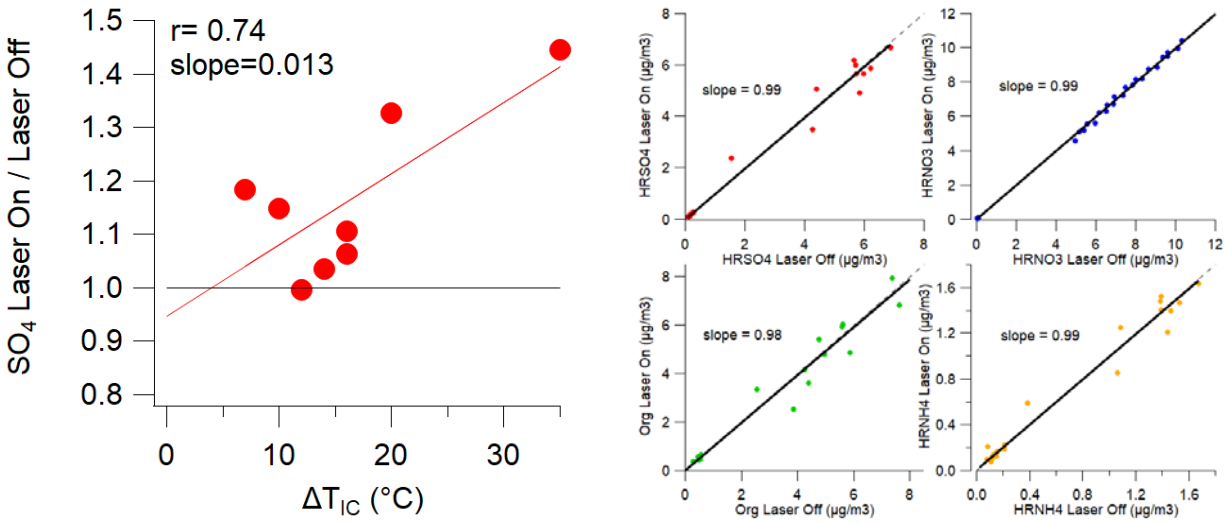


**Figure 25.** (Left) Ratio of SO4 signal laser on to laser off as a function of temperature change on the ionization chamber. (Right) Mass loading with laser on versus laser off for $SO_4$, $NO_3$, $NH_4$ and organic from laboratory generated particles.

After analyzing ten different baffle configurations, most were found to decrease the laser on/laser off temperature difference of the ion chamber to below 20 C. The left-hand panel in Figure 25 shows that decreasing the change in ionization chamber temperature significantly decreases the difference in $SO_4$ between laser on and laser off. The right-hand panel in Figure 25 shows that, for the best baffle configuration with < 10C change in the ionization chamber, the mass loading is the same for laser on and laser off for laboratory generated ammonium nitrate, ammonium sulfate and glutaric acid particles. Experiments are currently in progress to measure the laser on/laser off mass loading for ambient particles sampled from the roof of the Aerodyne building. These results will lead to better quantification of SP-AMS results when the instrument is operated with both vaporizers.

**Task 3. Model Development and Evaluation (Year 1 and Year 2)**

We started discussions with Dr. Zaveri about utilizing the SP-AMS and SP2 chemical information to model near-field biomass burning plumes using his MOSAIC model by helping to develop and evaluate new representations of SOA formation and BC mixing state evolution and their impact on CCN and optical properties for BBOP conditions. MOSAIC treats tropospheric trace gas photochemistry, nucleation, aerosol thermodynamics, kinetic gas-particle mass transfer of $H_2SO_4$, $HNO_3$, HCl and $NH_3$, particle-phase chemistry, coagulation, and sectional growth dynamics. It also predicts optical properties using the core-shell Mie theory and CCN activity using the Kappa-Kohler theory [*Zaveri et al.*, 2010]. A recent update includes a new framework for kinetic SOA partitioning that takes into account diffusion and chemical reaction within the particle phase, thereby capturing the complex interplay between the condensing species volatility, particle phase state (liquid, solid, or semisolid), particle-phase chemistry, and growth dynamics [*Zaveri et al.*, 2014]. The new framework allows the model to predict not just total SOA mass, but also its size distribution, which is crucial in determining the climate-relevant aerosol properties. The framework is computationally efficient and amenable for use in regional and global atmospheric models, and currently awaits specification of the various gas- and particle-phase chemistries and the related physicochemical properties that are important for SOA

formation from different precursors (including biomass burning emissions), under various atmospherically relevant conditions.

We also started discussions with Dr. Matthew Alvarado (AER, Inc.). Dr. Alvarado has DOE ASR funding to analyze BBOP data using his Aerosol Simulation Program (ASP) model to simulate the evolution of $O_3$ and secondary organic aerosol (SOA) within near-field biomass burning plumes [*Alvarado et al.*, 2015]. During detailed discussions at the spring 2016 DOE ASR meeting, we discussed with Dr. Alvarado how to (1) interact with us in terms of using and modeling the chemical information from the SP-AMS instrument during BBOP, (2) how to use his model to help guide our SP-AMS PMF analysis, using $O_3$ and other gas phase markers for comparisons with factors, and (3) how we can interact and build on our measurement-model relationship as we prepare to participate in the NOAA FIREX study over the next four years with our Aerodyne Mobile Laboratory (AML).

**c. Opportunities for Training/Professional Development**

This project provided opportunities for training for a graduate student at the University of Montana and training of a postdoctoral researcher at Aerodyne Research, Inc.. This project provided opportunities for professional development through conference attendance (American Association for Aerosol Research Annual Meeting, American Geophysical Union Fall Meeting, European Aerosol Conference, and International Conference on Carbonaceous Particles in the Atmosphere) and workshop participation (ASR Annual PI Science Meeting, and Aerodyne AMS Users Meeting).

**d. Dissemination of Results**

The results of this project were disseminated through conference presentations and through publications in archival journals.

**1.i. Journal publications**


Collier, S., S. Zhou, T. B. Onasch, D. A. Jaffe, L. Kleinman, A. J. Sedlacek, III, N. Briggs, J. Hee, E. Fortner, J. E. Shilling, D. Worsnop, R. J. Yokelson, C. Parworth, X. Ge, J. Xu, Z. Butterfield, D. Chand, M. K. Dubey, M. Pekour, S. Springston and Q. Zhang (2016). "Regional Influence of Aerosol Emissions from Wildfires Driven by Combustion Efficiency: Insights from the BBOP Campaign." Env. Sci. and Tech. **50**(16): 8613-8622.

Zhou, S., S. Collier, D. A. Jaffe, N. L. Briggs, J. Hee, A. J. Sedlacek III, L. Kleinman, T. B. Onasch and Q. Zhang (2017). "Regional influence of wildfires on aerosol chemistry in the western US and insights into atmospheric aging of biomass burning organic aerosol." Atmospheric Chemistry and Physics **17**(3): 2477-2493.

Liu, X., L. G. Huey, R. J. Yokelson, V. Selimovic, I. J. Simpson, M. Müller, J. L. Jimenez, P. Campuzano-Jost, A. J. Beyersdorf, D. R. Blake, Z. Butterfield, Y. Choi, J. D. Crounse, D. A. Day, G. S. Diskin, M. K. Dube, E. Fortner, T. F. Hanisco, W. Hu, L. E. King, L. Kleinman, S. Meinardi, T. Mikoviny, T. B. Onasch, B. B. Palm, J. Peischl, I. B. Pollack, T. B. Ryerso, G. W. Sachse, A. J. Sedlacek, III, J. E. Shilling, S. Springston, J. M. S. Clair, D. J. Tanner, A. P. Teng, P. O. Wennberg, A. Wisthaler and G. M. Wolfe (2017). "Airborne measurements of western US wildfire emissions: Comparison with prescribed burning and air quality implications." Journal of Geophysical Research: Atmospheres **122**(11): 6108-6129.

Sedlacek, A. J., III, P. R. Buseck, K. Adachi, T. Onasch, S. Springston and L. Kleinman (2018). "Formation and evolution of tar balls from northwestern US wildfires." Atmos. Chem. Phys **18**: 11289-11301.

Sedlacek, A. J., III, T. B. Onasch, L. Nichman, E. R. Lewis, P. Davidovits, A. Freedman and L. Williams (2018). "Formation of Refractory Black Carbon by SP2-Induced Charring of Organic Aerosol." Aerosol Science and Technology: doi: 10.1080/02786826.02782018.01531107.

Zhang, Q., S. Zhou, S. Collier, D. Jaffe, T. Onasch, J. Shilling, L. Kleinman and A. Sedlacek (2018). Understanding Composition, Formation, and Aging of Organic Aerosols in Wildfire Emissions via Combined Mountain Top and Airborne Measurements. Biomass Burning Organic Aerosol, ACS**:** in press.

Onasch, T. B., J. Shilling, A. J. Sedlacek, III, E. Fortner, M. Pekour, D. Chand, A. Freedman1, S. Zhou, S. Collier, Q. Zhang, L. Kleinman, J. Wormhoudt, D. Worsnop, R. Yokelson, K. Adachi, P. Buseck and L. Williams (2018). "Chemical composition and optical properties of wildland and agricultural biomass burning particles measured downwind during BBOP study." Atmos. Chem. Phys: in preparation.

Sedlacek, A. J., III, L. Kleinman, W. P. Arnott, T. Onasch, S. R. Springston, S. Smith and S. Oatis (2018). "Attribution of Aerosol Light Absorption in Wildfires " Atmos. Chem. Phys: in preparation.

Adachi, K., A. J. Sedlacek, III, L. Kleinman, J. Wang, D. Chand, J. M. Hubbe, T. B. Onasch, T. Kinase, K. Sakata, Y. Takahashi and P. R. Buseck (2018). "Formation of tarballs though the aging of liquid organic particles from biomass burning." Nature Geoscience: in preparation.

Sedlacek, A. J., III, T. B. Onasch, L. I. Kleinman, K. Adachi, W. P. Arnott, P. R. Buseck, S. Collier, E. Fortner, A. Freedman, D. Jaffe, M. Pekour, J. Shilling, R. J. Yokelson, Q. Zhang and S. Zhou (2018). "Biomass Burning Observation Project: Investigating the Near-Field Evolution of Aerosols from Wildfires." Bulletin of the American Meteorological Society: in prepration.

**1.iii. Other publications, conference papers and presentations**

Final Report: Kleinman, L. and A. J. Sedlacek, III (2016). Biomass Burning Observation Project (BBOP) Final Campaign Summary. DOE/SC-ARM-15-083.

Poster Presentation: Chemical composition and optical properties of wildland and agricultural biomass burning particles measured downwind during BBOP study, Timothy Onasch, John Shilling, Edward Fortner, Mikhail Pekour, Andrew Freedman, Larry Kleinman, Arthur Sedlacek, Duli Chand, Douglas Worsnop, 2015 Joint User Facility and PI Science Team Meeting, Vienna, VA, March, 2015.

Poster Presentation: Evolution of Biomass Burning Optical Properties in the Near-Field, A.J. Sedlacek, III, W. P. Arnott, D. Chand, E. Fortner, A. Freedman, L. Kleinman, T. B. Onasch, S. R. Springston, and S. Smith, 2015 Joint User Facility and PI Science Team Meeting, Vienna, VA, March, 2015.

Poster Presentation: Time Evolution of Biomass Burning Plumes Observed in BBOP, L. Kleinman, A.J Sedlacek lll, R. Yokelson, T. Onasch, E. Fortner, K. Adachi, P.B. Buseck, D. Chand, M.V. Dubey, J. Shilling, S. Springston, J. Wang, R. Zaveri, Q. Zhang, 2015 Joint User Facility and PI Science Team Meeting, Vienna, VA, March, 2015.

Oral Presentation: Evolution of Tar Balls, Peter Buseck, Kouji Adachi, Larry Kleinman, Timothy B. Onasch, Arthur J. Sedlacek, III, 2015 Joint User Facility and PI Science Team Meeting, Vienna, VA, March, 2015.

Oral Presentation: Chemical composition of wildland and agricultural biomass burning particles measured downwind during BBOP study, Timothy Onasch, John Shilling, Edward

Fortner, Mikhail Pekour, Duli Chand, Andrew Freedman, S. Collier, Q. Zhang, Larry Kleinman, Arthur Sedlacek, Douglas Worsnop, abstract 1AAS_P001, European Aerosol Conference, Milan, Italy, September, 2015.

Oral Presentation: Evolution of Biomass Burning Aerosol Optical Properties in the Near Field, A. J. Sedlacek and L. Kleinman, P. Arnott, K. Adachi, P. Buseck, D. Chand, E. Fortner, A. Freedman, T. Onasch, J. Shilling, S. Smith, S. R. Springston, J. Wang, R. Yokelson, 11th International Conference on Carbonaceous Particles in the Atmosphere, Berkeley, CA, August, 2015.

Poster Presentation: Chemical composition of wildland and agricultural biomass burning particles measured downwind during BBOP study, Timothy Onasch, John Shilling, Arthur Sedlacek, Edward Fortner, Mikhail Pekour, Duli Chand, Andrew Freedman, Shan Zhou, S. Collier, Q. Zhang, Larry Kleinman, Joda Wormhoudt, Douglas Worsnop, Robert Yokelson, Kouji Adachi, Peter Buseck, Leah Williams, ARM Climate Research Facility and ASR Program Joint User Facility/Principal Investigator Meeting, Vienna, VA, May, 2016.

Oral Presentation: Chemical composition and optical properties of wildland and agricultural biomass burning particles measured downwind during BBOP study, Timothy Onasch, John Shilling, Arthur Sedlacek, Edward Fortner, Mikhail Pekour, Duli Chand, Andrew Freedman, Shan Zhou, S. Collier, Q. Zhang, Larry Kleinman, Joda Wormhoudt, Douglas Worsnop, Robert Yokelson, Kouji Adachi, Peter Buseck, Leah Williams, ARM Climate Research Facility and ASR Program Joint User Facility/Principal Investigator Meeting, Vienna, VA, May, 2016.

Poster Presentation: Chemical composition and optical properties of wildland and agricultural biomass burning particles measured downwind during BBOP study, Timothy Onasch, John Shilling, Joda Wormhoudt, Arthur Sedlacek, Edward Fortner, Mikhail Pekour, Duli Chand, Shan Zhou, S. Collier, Q. Zhang, Larry Kleinman, Ernie Lewis, Douglas Worsnop, Robert Yokelson, Kouji Adachi, Peter Buseck, Andrew Freedman and Leah Williams, ARM Climate Research Facility and ASR Program Joint User Facility/Principal Investigator Meeting, Vienna, VA, March 2017.

Poster Presentation: Tar balls observed in wildfire plumes are weakly absorbing secondary aerosol, Arthur Sedlacek, Peter Buseck, Kouji Adachi, Larry Kleinman, Timothy Onasch, Stephen Springston, ARM Climate Research Facility and ASR Program Joint User Facility/Principal Investigator Meeting, Vienna, VA, March 2017.

Oral Presentation: Regional Influences of Wildfires on Atmospheric Aerosol in the Western US and Insights into Emission and Aging of Biomass Burning Organic Aerosol, Q. Zhang, S. Zhou, S. Collier, D. Jaffe, J. Hee, N. Wigder, T. Onasch, L. Kleinman, and A. Sedlacek, European Aerosol Conference, Zurich, Switzerland, August, 2017.

Poster Presentation: Near-field changes to the optical and chemical properties of biomass burning particles, T. B. Onasch, J. Wormhoudt, A. Sedlacek, L. Kleinman, E. Fortner, J. Shilling, M. Pekour, D. Chand, S. Collier, Q. Zhang, R. Yokelson, K. Adachi, P. Buseck, L. Williams, A. Freedman, European Aerosol Conference, Zurich, Switzerland, August, 2017.

Oral Presentation: 1AC.1 Properties and Evolution of Biomass Burning Organic Aerosol from Wildfires in the Western U.S. Shan Zhou, Sonya Collier, Timothy Onasch, Daniel Jaffe, Lawrence Kleinman, Arthur J. Sedlacek, Qi Zhang, American Association for Aerosol Research Annual Meeting, Raleigh, NC, October 2017.

Oral Presentation: A34D-07 Emission and Aging of Organic Aerosol in Wildfires in the Western US: Insights from the DOE BBOP Campaign, Qi Zhang, Shan Zhou, Sonya Collier, Dan A Jaffe, Timothy Bruce Onasch, Lawrence I Kleinman, Arthur J Sedlacek III, AGU Fall Meeting, New Orleans, MS, December 2017.

Oral Presentation: A34D-06 Tar balls are processed, weakly absorbing, primary aerosol particles formed downwind of boreal forest fires, Arthur J Sedlacek III, Peter R Buseck, Kouji Adachi, Lawrence I Kleinman, Timothy Bruce Onasch, Stephen R. Springston, AGU Fall Meeting, New Orleans, MS, December 2017.

Poster Presentation: A43E-1453 Time Dependence of Aerosol Light Scattering Downwind of Forest Fires, Lawrence I Kleinman, Arthur J Sedlacek III, Jian Wang, Ernie R Lewis, Stephen R. Springston, Duli Chand, John Shilling, William P Arnott, Andrew Freedman, Timothy Bruce Onasch, Edward Fortner, Qi Zhang, Robert J Yokelson, Kouji Adachi and Peter R Buseck, AGU Fall Meeting, New Orleans, MS, December 2017.

Poster Presentation: A43E-1451 Chemical composition of wildland and agricultural biomass burning particles measured downwind during the BBOP study, Timothy Bruce Onasch, John E Shilling, Joda Wormhoudt, Arthur J Sedlacek III, Edward Fortner, Mikhail S Pekour, Duli Chand, Shan Zhou, Sonya Collier, Qi Zhang, Lawrence I Kleinman, Ernie R Lewis, Robert J Yokelson, Kouji Adachi, Peter R Buseck, Andrew Freedman and Leah R Williams, AGU Fall Meeting, New Orleans, MS, December 2017.

Poster Presentation: Chemical composition of wildland and agricultural biomass burning particles measured downwind during the BBOP study, Timothy Onasch, John Shilling, Joda Wormhoudt, Arthur Sedlacek, Edward Fortner, Mikhail Pekour, Duli Chand, Shan Zhou, Sonya Collier, Qi Zhang, Larry Kleinman, Ernie R. Lewis, Robert Yokelson, Kouji Adachi, Peter Buseck, Andrew Freedman, Leah Williams, ARM Climate Research Facility and ASR Program Joint User Facility/Principal Investigator Meeting, Vienna, VA, March, 2018.

Poster Presentation: 7IM.14 Particle Detection Using the Dual-vaporizer Configuration of the Soot Particle Aerosol Mass Spectrometer, Anita Avery, Edward Fortner, Leah Williams, Wade Robinson, Timothy Onasch, International Aerosol Conference, St. Louis, MO, September 2018.

Oral Presentation: 13CA.2 Chemical composition of Biomass Burning Particles Measured with a Soot Particle Aerosol Mass Spectrometer Downwind during the BBOP Study, Timothy Onasch, Anita Avery, John Shilling, Joda Wormhoudt, Arthur J. Sedlacek, Edward Fortner, Michail Pekour, Shan Zhou, Sonya Collier, Qi Zhang, Lawrence Kleinman, Ernie Lewis, Andrew Freedman and Leah Williams, International Aerosol Conference, St. Louis, MO, September 2018.

Oral Presentation: A52C-01 Aerosol Particle Changes in the Atmosphere and their Effects on Optical Properties and Climate, Peter R Buseck, Kouji Adachi, Lawrence I Kleinman, Timothy Bruce Onasch, Arthur J Sedlacek III, AGU Fall Meeting, Washington D.C., December 2018.

Poster Presentation: A43K-3198 Formation and chemical properties of tar balls from biomass burning, Kouji Adachi, Arthur J Sedlacek III, Lawrence I Kleinman, Timothy Bruce Onasch, Stephen R. Springston, and Peter R Buseck, AGU Fall Meeting, Washington D.C., December 2018.

Poster Presentation: A33L-3364 Formation of Refractory Black Carbon by SP2-Induced Charring of Organic Aerosol, Arthur J Sedlacek III, Timothy Bruce Onasch, Leonid

Nichman, Ernie R Lewis, Paul Davidovits, Andrew Freedman and Leah R Williams, AGU Fall Meeting, Washington D.C., December 2018.

**Cost Status**

**Table 4.** Approved costs for Year 1 and Year 2 and funds spent in each year.

| | | BUDGET Year 1 | SPENT Year 1 | BUDGET Year 2 | SPENT Year 2 | SPENT Year 3 | CUMULATIVE SPENT |
|---|---|---|---|---|---|---|---|
| START DATE | | 15-Aug | 15-Aug | 16-Aug | 16-Aug | 17-Aug | 15-Aug |
| END DATE | | 16-Jul | 16-Jul | 17-Jul | 17-Jul | 18-Jul | 18-Jul |
| | RATE | COST | | | | | |
| Total Labor | | 42,503 | 47,747 | 40,190 | 22,302 | 11,283 | 81,332 |
| Subcontracts: | | 95,000 | 51,500 | 95,000 | 69,776 | 68,724 | 190,000 |
| Matls & Supplies | | 2,300 | 4,675 | 2,300 | 3,413 | 3,028 | 11,116 |
| Services | | | 221 | | 737 | 145 | 1,103 |
| Patent Costs | | | | | | | |
| **Total Direct Costs** | | **139,135** | **104,143** | **142,382** | **96,228** | **83,180** | **283,551** |
| | | | | | | | |
| Labor Overhead | 140% | 59,504 | 66,845 | 56,266 | 31,224 | 15,796 | 113,865 |
| G&A Base | | 198,639 | 170,987 | 198,648 | 127,453 | 98,980 | 397,420 |
| General & Administration | 15% | 29,796 | 25,648 | 29,797 | 19,118 | 14,847 | 59,613 |
| **Total Indirect Costs** | | **179,864** | **92,493** | **180,450** | **50,342** | **30,643** | **173,478** |
| | | | | | | | |
| **Total Costs** | | **228,435** | **196,636** | **228,445** | **146,570** | **113,823** | **457,029** |

**References**


Adachi, K., et al. (2018), Formation of tarballs though the aging of liquid organic particles from biomass burning, *Nature Geoscience*, in preparation.

Akagi, S. K., et al. (2013), Measurements of reactive trace gases and variable O3 formation rates in some South Carolina biomass burning plumes, *Atmos. Chem. Phys.*, *13*(3), 1141-1165, doi:10.5194/acp-13-1141-2013.

Alvarado, M., C. Lonsdale, R. Yokelson, S. K. Akagi, H. Coe, J. Craven, E. Fischer, G. McMeeking, J. Seinfeld, and T. Soni (2015), Investigating the links between ozone and organic aerosol chemistry in a biomass burning plume from a prescribed fire in California chaparral, *Atmos. Chem. Phys.*, *15*(12), 6667-6688.

Burling, I. R., R. J. Yokelson, S. K. Akagi, S. P. Urbanski, C. E. Wold, D. W. T. Griffith, T. J. Johnson, J. Reardon, and D. R. Weise (2011), Airborne and ground-based measurements of the trace gases and particles emitted by prescribed fires in the United States, *Atmos. Chem. Phys.*, *11*(23), 12197-12216, doi:10.5194/acp-11-12197-2011.

Cappa, C. D., et al. (2012), Radiative absorption enhancements due to the mixing state of atmospheric black carbon, *Science*, *337*(6098), 1078-1081.
Chakrabarty, R. K., H. Moosmüller, L.-W. A. Chen, K. Lewis, W. P. Arnott, C. Mazzoleni, M. K. Dubey, C. E. Wold, W. M. Hao, and S. M. Kreidenweis (2010), Brown carbon in tar balls from smoldering biomass combustion, *Atmos. Chem. Phys.*, *10*(13), 6363–6370, doi:6310.5194/acp-6310-6363-2010.
Collier, S., et al. (2016), Regional Influence of Aerosol Emissions from Wildfires Driven by Combustion Efficiency: Insights from the BBOP Campaign, *Environ. Sci. Tech.*, *50*(16), 8613-8622.
Corbin, J., B. Sierau, M. Gysel, M. Laborde, A. Keller, J. Kim, A. Petzold, T. Onasch, U. Lohmann, and A. Mensah (2014), Mass spectrometry of refractory black carbon particles from six sources: carbon-cluster and oxygenated ions, *Atmos. Chem. Phys.*, *14*(5), 2591-2603.
Cubison, M. J., et al. (2011), Effects of aging on organic aerosol from open biomass burning smoke in aircraft and laboratory studies, *Atmos. Chem. Phys.*, *11*(23), 12049-12064, doi:12010.15194/acp-12011-12049-12011.
Dingle, J. H., et al. (2016), Aerosol Optical Extinction during the Front Range Air Pollution and Photochemistry Éxperiment (FRAPPÉ) 2014 Summertime Field Campaign, Colorado U.S.A, *Atmos. Chem. Phys. Discuss.*, *2016*, 1-21, doi:10.5194/acp-2016-211.
Feng, Y., V. Ramanathan, and V. R. Kotamarthi (2013), Brown carbon: a significant atmospheric absorber of solar radiation?, *Atmos. Chem. Phys.*, *13*(17), 2795–2833, doi:2710.5194/acp-2713-8607-2013.
Hecobian, A., et al. (2011), Comparison of chemical characteristics of 495 biomass burning plumes intercepted by the NASA DC-8 aircraft during the ARCTAS/CARB-2008 field campaign, *Atmos. Chem. Phys.*, *11*(24), 13325-13337, doi:10.5194/acp-11-13325-2011.
Hennigan, C. J., M. A. Miracolo, G. J. Engelhart, A. A. May, A. A. Presto, T. Lee, A. P. Sullivan, G. R. McMeeking, H. Coe, and C. E. Wold (2011), Chemical and physical transformations of organic aerosol from the photo-oxidation of open biomass burning emissions in an environmental chamber, *Atmos. Chem. Phys.*, *11*(15), 7669-7686.
Kleinman, L., and A. J. Sedlacek, III (2016), Biomass Burning Observation Project (BBOP) Final Campaign Summary*Rep.*, DOE/SC-ARM-15-083 pp, Office of Science, US Department of Energy.
Kroll, J. H., et al. (2011), Carbon oxidation state as a metric for describing the chemistry of atmospheric organic aerosol, *Nature Chemistry*, *3*(2), 133-139.
Liu, S., et al. (2014), Aerosol single scattering albedo dependence on biomass combustion efficiency: Laboratory and field studies, *Geophys. Res. Lett.*, *41*, 742–748, doi:710.1002/2013GL058392.
Liu, S., et al. (2015), Enhanced light absorption by mixed source black and brown carbon particles in UK winter, *Nature Communications*, *6*(8435), doi: 10.1038/ncomms9435.
Liu, X., et al. (2017), Airborne measurements of western US wildfire emissions: Comparison with prescribed burning and air quality implications, *J. Geophys. Res. Atmos.*, *122*(11), 6108-6129.
Lobert, J. M., D. H. Scharffe, W. M. Hao, T. A. Kuhlbusch, R. Seuwan, P. Warneck, and P. J. Crutzen (1991), Experimental evaluation of biomass burning emissions: nitrogen and carbon containing compounds, in *Global Biomass Burning: Atmospheric, Climatic and*

*Biospheric Implications*, edited by J. S. Levine, pp. 289-304, MIT Press, Cambridge, MA.

Massoli, P., et al. (2012), Pollution Gradients and Chemical Characterization of Particulate Matter from Vehicular Traffic near Major Roadways: Results from the 2009 Queens College Air Quality Study in NYC, *Aerosol Sci. Tech.*, *46*(11), 1201-1218, doi:DOI: 10.1080/02786826.2012.701784.

Massoli, P., P. L. Kebabian, T. B. Onasch, F. B. Hills, and A. Freedman (2010), Aerosol Light Extinction Measurements by Cavity Attenuated Phase Shift (CAPS) Spectroscopy: Laboratory Validation and Field Deployment of a Compact Aerosol Particle Extinction Monitor *Aerosol Sci. Tech.*, *44*(6), 428-435.

May, A. A., T. Lee, G. R. McMeeking, S. Akagi, A. P. Sullivan, S. Urbanski, R. J. Yokelson, and S. M. Kreidenweis (2015), Observations and analysis of organic aerosol evolution in some prescribed fire smoke plumes, *Atmos. Chem. Phys.*, *15*(11), 6323–6335, doi:6310.5194/acp-6315-6323-2015.

McMeeking, G. R., S. M. Kreidenweis, S. Baker, C. M. Carrico, J. C. Chow, J. L. Collett, W. M. Hao, A. S. Holden, T. W. Kirchstetter, and W. C. Malm (2009), Emissions of trace gases and aerosols during the open combustion of biomass in the laboratory, *J. Geophys. Res. Atmos.*, *114*(D19).

Müller, M., et al. (2016), In situ measurements and modeling of reactive trace gases in a small biomass burning plume, *Atmos. Chem. Phys.*, *16*, 3813-3824, doi:3810.5194/acp-3816-3813-2016.

Ng, N. L., M. R. Canagaratna, J. L. Jiménez, P. S. Chhabra, J. H. Seinfeld, and D. R. Worsnop (2011), Changes in organic aerosol composition with aging inferred from aerosol mass spectra, *Atmos. Chem. Phys.*, *11*(13), 6465–6474, doi:6410.5194/acp-6411-6465-2011.

Onasch, T. B., et al. (2015a), Investigations of SP-AMS Carbon Ion Distributions as a Function of Refractory Black Carbon Particle Type, *Aerosol Sci. Tech.*, *49*(6), 409-422, doi:10.1080/02786826.2015.1039959.

Onasch, T. B., P. Massoli, P. L. Kebabian, F. B. Hills, F. W. Bacon, and A. Freedman (2015b), Single scattering albedo monitor for airborne particulates, *Aerosol Sci. Tech.*, *49*(4), 267-279.

Onasch, T. B., et al. (2018), Chemical composition and optical properties of wildland and agricultural biomass burning particles measured downwind during BBOP study, *Atmos. Chem. Phys*, in preparation.

Onasch, T. B., A. Trimborn, E. C. Fortner, J. T. Jayne, G. L. Kok, L. R. Williams, P. Davidovits, and D. Worsnop (2012), Soot Particle Aerosol Mass Spectrometer: Development, Validation, and Initial Application, *Aerosol Sci. Tech.*, *46*(7), 804-817, doi:DOI:10.1080/02786826.2012.663948.

Pósfai, M., A. Gelencsér, R. Simonics, K. Arato, J. Li, P. V. Hobbs, and P. R. Buseck (2004), Atmospheric tar balls: Particles from biomass and biofuel burning, *J. Geophys. Res.*, *109*(D6), D06213, doi:06210.01029/02003JD004169.

Saleh, R. C. J. H., G. R. McMeeking, W. K. Chuang, E. S. Robinson, H. Coe, N. M. Donahue, and A. L. Robinson (2013), Absorptivity of brown carbon in fresh and photo-chemically aged biomass-burning emissions, *Atmos. Chem. Phys.*, *13*, 7683–7693, doi:7610.5194/acp-7613- 7683-2013

Schwarz, J. P., et al. (2010), The Detection Efficiency of the Single Particle Soot Photometer, *Aerosol Sci. Tech.*, *44*(8), 612–628, doi:610.1080/02786826.02782010.02481298.

Sedlacek, A. J., III, P. R. Buseck, K. Adachi, T. Onasch, S. Springston, and L. Kleinman (2018a), Formation and evolution of tar balls from northwestern US wildfires, *Atmos. Chem. Phys*, *18*, 11289-11301.

Sedlacek, A. J., III, L. Kleinman, W. P. Arnott, T. Onasch, S. R. Springston, S. Smith, and S. Oatis (2018b), Attribution of Aerosol Light Absorption in Wildfires *Atmos. Chem. Phys*, in preparation.

Sedlacek, A. J., III, E. R. Lewis, T. B. Onasch, A. T. Lambe, and P. Davidovits (2015), Investigation of Refractory Black Carbon-Containing Particle Morphologies Using the Single-Particle Soot Photometer (SP2), *Aerosol Sci. Tech.*, *49*(10), 872–885, doi:810.1080/02786826.02782015.01074978.

Sedlacek, A. J., III, T. B. Onasch, L. Nichman, E. R. Lewis, P. Davidovits, A. Freedman, and L. Williams (2018c), Formation of Refractory Black Carbon by SP2-Induced Charring of Organic Aerosol, *Aerosol Sci. Tech.*, doi: 10.1080/02786826.02782018.01531107.

Stocker, T. F., D. Qin, G.-K. Plattner, M. Tignor, S. K. Allen, J. Boschung, A. Nauels, Y. Xia, V. Bex, and P. M. Midgley (2013), *Climate change 2013: The physical science basis*, IPCC, Cambridge University Press, New York.

Tóth, A., A. Hoffer, I. Nyirő-Kósa, M. Pósfai, and A. Gelencsér (2014), Atmospheric tar balls: aged primary droplets from biomass burning?, *Atmos. Chem. Phys.*, *14*(13), 6669-6675.

Wiedinmyer, C., S. K. Akagi, R. J. Yokelson, L. K. Emmons, J. A. Al-Saadi, J. J. Orlando, and A. J. Soja (2011), The Fire INventory from NCAR (FINN): a high resolution global model to estimate the emissions from open burning, *Geosci. Model Dev.*, *4*(3), 625-641, doi:10.5194/gmd-4-625-2011.

Yokelson, R. J., I. R. Burling, S. P. Urbanski, E. L. Atlas, K. Adachi, P. R. Buseck, C. Wiedinmyer, S. K. Akagi, D. W. Toohey, and C. E. Wold (2011), Trace gas and particle emissions from open biomass burning in Mexico, *Atmospheric Chemistry and Physics*, *11*(14), 6787-6808, doi:10.5194/acp-11-6787-2011.

Yokelson, R. J., D. W. T. Griffith, and D. E. Ward (1996), Open-path Fourier transform infrared studies of large-scale laboratory biomass fires, *Journal of Geophysical Research: Atmospheres*, *101*(D15), 21067-21080, doi:10.1029/96JD01800.

Zaveri, R. A., J. C. Barnard, R. C. Easter, N. Riemer, and M. West (2010), Particle-resolved simulation of aerosol size, composition, mixing state, and the associated optical and cloud condensation nuclei activation properties in an evolving urban plume, *J. Geophys. Res.*, *115*, D17210, doi:17210.11029/12009JD013616.

Zaveri, R. A., R. C. Easter, J. E. Shilling, and J. H. Seinfeld (2014), Modeling kinetic partitioning of secondary organic aerosol and size distribution dynamics: representing effects of volatility, phase state, and particle-phase reaction, *Atmos. Chem. Phys.*, *14*(10), 5153-5181.

Zhou, S., S. Collier, D. A. Jaffe, N. L. Briggs, J. Hee, A. J. Sedlacek III, L. Kleinman, T. B. Onasch, and Q. Zhang (2017), Regional influence of wildfires on aerosol chemistry in the western US and insights into atmospheric aging of biomass burning organic aerosol, *Atmos. Chem. Phys.*, *17*(3), 2477-2493.